An Essential Adaptor for Apicoplast Fission and Inheritance in Malaria Parasites

Authors:

James Blauwkamp[1], Krithika Rajaram[2, 3], Sophia R. Staggers[4], Oliver Harrigan[1], Emma H. Doud[5], Sean T. Prigge[2], Stella Y. Sun[4], Sabrina Absalon[1#]

Affiliations:

[1]Indiana University School of Medicine, Department of Pharmacology and Toxicology, Indianapolis

[2]Johns Hopkins Bloomberg School of Public Health, Department of Molecular Microbiology and Immunology, Baltimore

[3]The Ohio State University College of Arts and Sciences, Department of Microbiology, Columbus

[4]University of Pittsburgh, Department of Structural Biology, Pittsburgh

[5]Biochemistry and Molecular Biology, Indiana University School of Medicine, Indianapolis

[#]Corresponding Author

Corresponding Author Email:

sabsalon@iu.edu

Abstract

Blood-stage *Plasmodium falciparum* parasites rely on a non-photosynthetic plastid, the apicoplast, for survival, making it an attractive target for antimalarial intervention. Like the mitochondrion, the apicoplast cannot be generated *de novo* and must be inherited by daughter parasites during cell division. This inheritance relies on coordinated apicoplast positioning and fission, but the molecular mechanisms controlling these processes remain poorly understood. Here, we identify a previously uncharacterized *P. falciparum* protein (Pf3D7_0613600), which we name PfAnchor, as a key regulator of apicoplast fission. Using Ultrastructure Expansion Microscopy (U-ExM), we show that PfAnchor localizes to the apicoplast throughout the asexual blood-stage. Conditional depletion disrupts apicoplast fission, leading to incomplete cytokinesis and parasite death. Notably, loss of the apicoplast's elongated branched structure via azithromycin treatment rescues these defects, underscoring Anchor's specific role in apicoplast fission. Immunoprecipitation identified an interaction with the dynamin-like GTPase PfDyn2, a key mediator of both apicoplast and mitochondrial fission, establishing PfAnchor as the first apicoplast-specific dynamin adaptor protein. Our findings define PfAnchor as an essential factor for apicoplast fission and inheritance in *P. falciparum* blood-stage parasites, highlighting parasite-specific organelle division as a potential vulnerability for therapeutic intervention.

Introduction

Protists, a diverse group of predominantly single-celled eukaryotes, represent the largest component of eukaryotic diversity and are found in nearly every environment [1, 2]. Like other eukaryotes, most protists contain mitochondria and/or plastid-derived organelles that support essential metabolic processes. Examples include photosynthetic plastids in dinoflagellates and the non-photosynthetic apicoplast found in most apicomplexan parasites [3]. Both mitochondria and plastids originate from endosymbiotic events where ancestral eukaryotes engulfed bacteria or algae that evolved into organelles [4]. Evidence for this evolutionary origin includes the presence of organelle genomes within mitochondria and

plastids, as well as the multi-membrane structure of plastids derived from secondary endosymbiosis [5]. Given their fundamental roles in survival and metabolism and the absence of plastids in human hosts, these organelles represent attractive targets for novel antiparasitic drug development [6, 7].

Malaria is a parasitic disease caused by protozoan *Plasmodium* parasites, with an estimated 249 million cases and 608,000 deaths reported in 2022 [8]. *Plasmodium* parasites invade host red blood cells and undergo multiple rounds of asynchronous DNA replication within a shared cytoplasm, resulting in a multi-nucleated parasite [9]. These parasites contain a non-photosynthetic plastid known as the apicoplast. This metabolic organelle is thought to have originated from a secondary endosymbiosis event involving red algae and possesses its own reduced genome of approximately 35kb [10-12]. While the apicoplast plays a role in fatty acid and heme synthesis, studies have shown that its essential functions include the synthesis of isoprenoid precursors such as isopentenyl pyrophosphate (IPP) and coenzyme A (CoA) [13-19].

The apicoplast in *Plasmodium* is a single, branching organelle that expands in volume as the parasite progresses through the intraerythrocytic cycle. Volume electron microscopy (EM) studies, along with our recent work using ultrastructure expansion microscopy (U-ExM), have confirmed that the apicoplast undergoes multiple asynchronous fission events during schizogony, coinciding with parasite cytokinesis [20-22]. Recent studies have shown that apicoplast fission is mediated by a dynamin-like protein, PfDyn2 (Pf3D7_1037500), and is essential for parasite survival, as the apicoplast cannot be synthesized de novo [23, 24]. Unlike classical dynamin proteins, which contain a pleckstrin homology (PH) domain for direct membrane interaction during fission, dynamin-related proteins rely on adaptor proteins to recruit them to membranes and assemble functional fission complexes [25-27]. Mitochondrial fission adaptors vary widely in sequence and structure, with four identified in humans [28-31], three in yeast [32-34], two in the related parasite *Toxoplasma gondii* [35, 36], and one in *Plasmodium* [37]. However, no adaptor proteins specific to apicoplast fission have been identified in either *T. gondii* or *P. falciparum*, leaving the mechanism by which PfDyn2 facilitates apicoplast division unresolved.

80 In this study, we identify and characterize PfAnchor (Pf3D7_0613600), a nuclear-
81 encoded protein that localizes to the apicoplast during the blood stage developmental
82 cycle. Using the inducible TetR-DOZI conditional knockdown system [38], we demonstrate
83 that PfAnchor is essential for parasite growth. Live microscopy of PfAnchor-deficient
84 parasites revealed that while egress occurs, daughter cells form large clumps, preventing
85 successful invasion. U-ExM analysis further showed that the apicoplast fails to undergo
86 proper fission, resulting in most daughter parasites remaining tethered to each other via a
87 collapsed apicoplast, while a subset of parasites emerges without an apicoplast. Blocking
88 apicoplast branching via azithromycin treatment fully rescued the growth defect in
89 PfAnchor-deficient parasites. Immunoprecipitation experiments identified an interaction
90 between PfAnchor and PfDyn2, suggesting that PfAnchor acts as a dynamin adaptor protein
91 required for apicoplast fission and inheritance. By uncovering a key regulator of apicoplast
92 division, this study provides new insights into the molecular machinery governing organelle
93 inheritance. Additionally, we highlight the potential of targeting apicoplast morphology as a
94 novel strategy for inducing same-cycle parasite death, positioning PfAnchor as a promising
95 therapeutic target for malaria intervention.

96

97 **Results**

98 **PfAnchor: A conserved *Plasmodium* apicoplast-associated protein in the blood stage.**

99 Proximal labeling experiments using *P. falciparum* Minichromosome Maintenance-
100 binding protein (PfMCMBP) as bait [39] led to the identification of an uncharacterized protein
101 that we named PfAnchor (Pf3D7_0613600, **Figure S1-S2, Supp Data 1**). PfAnchor is a
102 *Plasmodium specific* 1034 amino acid protein. No homologs of PfAnchor could be identified
103 in other apicomplexan organisms, suggesting it may represent a lineage-specific adaptation.
104 The sequence structure contains a hydrophobic helix at the N-terminal end, predicted to be
105 a transmembrane domain, as well as a potential phosphorylation site at S204 (**Figure 1a**).
106 Alphafold3 structure prediction [40] revealed an ordered region at the C-terminal end which
107 is present across *Plasmodium* species (**Figure 1a, Figure S3**). By combining Alphafold3

108 predictions with a DALI search [41], we, along with a recent publication [42], identified this
109 region as a putative pleckstrin homology (PH) domain (**Figure 1a**). These domains are
110 typically involved in membrane binding suggesting that PfAnchor may associate with a
111 membrane. Sequence analysis of the predicted PH domain revealed strong conservation
112 among *Plasmodium* species, with the highest similarity between *P. falciparum* and the
113 *Laverania* subgenus (**Figure S3a**). Alphafold3 structure predictions across *Plasmodium*
114 species with varying degrees of PfAnchor homology showed structural conservation of the
115 predicted PH domain with high confidence model prediction in multiple species (**Figure**
116 **S3b**). This structural conversation suggests that the predicted PH domain may have a
117 conserved functional role in *Plasmodium* parasites.

118 Having identified PfAnchor as a potential membrane-associated protein through
119 structural predictions, we next investigated its subcellular localization and membrane
120 association. To enable detection and conditional regulation of PfAnchor, we engineered a C-
121 terminal fusion of the protein with the spaghetti monster-V5 (smV5) epitope tag [43] and
122 integrated the TetR-based conditional knockdown system [38] into the 3D7 parasite strain,
123 named PfAnchor iKD (**Figure 1b, Figure S4**). This system allows for controlled expression of
124 PfAnchor in the presence of anhydrotetracycline (aTC), a small molecule that stabilizes
125 mRNA translation. In the absence of aTC, translation is suppressed, resulting in effective
126 protein knockdown. Although PfAnchor's transcriptional profile [44] suggests expression
127 throughout the entire intraerythrocytic developmental cycle (IDC), we detected protein
128 expression only from the trophozoite stage through segmented schizonts using western blot
129 analysis (**Figure 1c**). To validate the functionality of the inducible knockdown system, we
130 washed out aTC one cycle prior to analysis, approximately 10 hours before egress, and
131 collected samples 40 hours post-invasion. Western blot analysis showed that PfAnchor
132 expression was reduced by more than 90% across four independent biological replicates,
133 confirming the efficacy of the knockdown system (**Figure 1d**).

134 To determine whether PfAnchor is membrane-associated, we conducted sodium
135 carbonate solubility assays. Parasites were hypotonically lysed to remove soluble cytosolic
136 proteins, followed by sequential extraction with sodium carbonate (to release peripherally

137 associated membrane proteins) and Triton-X100 (to solubilize integral membrane proteins).
138 The resulting fractions, including the supernatant and pellet, were analyzed by western blot
139 to assess the distribution of PfAnchor. Although minor cytosolic contamination was
140 detected in the sodium carbonate fraction, most of PfAnchor was enriched in this fraction,
141 consistent with a peripheral association with membranes (**Figure 2a**).

142 Given its membrane association, we next sought to identify the specific membrane
143 compartment with which PfAnchor associates. Using U-ExM, we observed that PfAnchor
144 localizes to regions containing non-nuclear DNA, suggesting a potential association with a
145 DNA-containing organelle. By staining PfAnchor parasites with MitoTracker, we showed that
146 PfAnchor did not co-localize with the mitochondrion (**Figure 2b**). As the apicoplast
147 possesses its own genome, we hypothesized that PfAnchor might localize to the apicoplast
148 during this stage. To test this, we generated a new cell line by tagging PfAnchor with smV5 in
149 the PfMev::Api-GFP background [45] that we named PfAnchor^{Mev} iKD (**Figure S5**). This strain
150 enables conditional disruption of the apicoplast by mevalonate (MVA) supplementation,
151 supporting viability of the parasite without the organelle. This system facilitates visualization
152 of the apicoplast through GFP tagging and allows investigation of PfAnchor's function in the
153 absence of an intact apicoplast. Imaging analysis of this cell line revealed that PfAnchor
154 localizes to the periphery of the apicoplast throughout schizogony (**Figure 2b, c**), supporting
155 its involvement in apicoplast biology.

156 To determine the orientation of PfAnchor within the apicoplast, we performed
157 proteinase K protection assays. Infected red blood cells were lysed with saponin to release
158 parasites, followed by treatment with digitonin to selectively permeabilize the parasite
159 plasma membrane. The resulting pellet was exposed to proteinase K to degrade cytosolic-
160 facing proteins while preserving proteins within organellar compartments. We found that
161 PfAnchor was susceptible to proteinase K digestion, indicating that its C-terminal epitope
162 tag faces the cytosol (**Figure 2d**). Together, these findings demonstrate that PfAnchor is a
163 cytosol-facing protein associated with the apicoplast membrane.

164

165 **PfAnchor is essential for apicoplast partitioning and merozoite formation.**

166 To investigate the role of PfAnchor in parasite development, we removed
167 anhydrotetracycline (aTC) from the culture and monitored parasite growth by microscopy.
168 PfAnchor-deficient parasites exhibited a complete growth arrest during the first cycle of
169 depletion, with no early-stage parasites detected in the culture, suggesting a critical role in
170 either egress or invasion (**Figure 3a**). To test this, we performed live microscopy on PfAnchor-
171 expressing and PfAnchor-deficient parasites to investigate whether egress was affected.
172 Parasites were treated with Compound 1 to arrest and synchronize them just prior to egress
173 from red blood cells [46]. After washing with fresh media, egress events were monitored.
174 PfAnchor-expressing parasites displayed rapid and explosive egress, with individual
175 daughter merozoites dispersing quickly. By contrast, PfAnchor-deficient parasites
176 underwent egress, yet the majority of daughter merozoites remained clustered and failed to
177 fully separate, often remaining attached near the food vacuole (**Figure 3b, c**). To quantify
178 egress phenotypes, we categorized parasites based on morphology: "normal" morphology
179 was defined as minimal merozoite clumping with daughter parasites dispersing effectively,
180 while "abnormal" morphology was characterized by limited separation of daughter
181 parasites, which formed slow-moving or immobile clumps. PfAnchor-expressing parasites
182 showed an average of 89.3 +/- 9.5% normal morphology (52/61 egress events) over three
183 biological replicates while PfAnchor-deficient parasites showed an average of 10.7 +/- 9.3%
184 normal morphology (3/39 egress events) over three biological replicates. We note that
185 PfAnchor-deficient parasite morphology closely resembles the phenotype associated with
186 impaired apicoplast segregation [47]. Given this resemblance, we hypothesized that
187 disrupted apicoplast branching may underline the observed cytokinesis defect. To test this,
188 we visualized the apicoplast morphology in PfAnchor-deficient parasites expressing ACP-
189 GFP (PfAnchor^{Mev} iKD parasites). Imaging of PfAnchor deficient parasites revealed two
190 distinct groups of merozoites: clumped merozoites that share a single, unsegregated
191 apicoplast, and free merozoites that display no apicoplast signal. We hypothesize that these
192 free merozoites lack an apicoplast. In contrast, in PfAnchor-expressing parasites exhibit
193 proper segregation, with each merozoite containing a distinct apicoplast (**Figure 3d**). These

194 findings demonstrate that PfAnchor is essential for apicoplast inheritance during merozoite
195 formation.

196 **PfAnchor is required for apicoplast division during IDC.**

197 Given its localization to the apicoplast periphery and the observed defects in
198 organelle inheritance upon knockdown, we reasoned that PfAnchor plays a direct role in
199 apicoplast division. We hypothesize that in the absence of PfAnchor, apicoplast fission fails,
200 resulting in merozoites tethered by a single, undivided apicoplast. To test this, we used U-
201 ExM to track apicoplast division during parasite replication and determine how PfAnchor
202 depletion disrupts organelle division and inheritance. To assess whether PfAnchor loss
203 affects apicoplast biogenesis, we measured apicoplast area in cell projections [21]. No
204 significant differences were observed between PfAnchor-expressing and deficient parasites,
205 indicating that apicoplast biogenesis remains unaffected (**Figure 4a**). Additionally, as we
206 and others previously demonstrated, the apicoplast adopts a characteristic crown shape
207 during early segmentation, with a single branched apicoplast connecting all outer centriolar
208 plaques (CPs) [21, 48, 49]. This organization was also observed in PfAnchor-deficient
209 parasites, indicating that the pre-fission positioning of the apicoplast and its association
210 with the CPs remain unaffected in the absence of PfAnchor (**Figure S6**). However, PfAnchor-
211 deficient parasites exhibited a striking defect in apicoplast inheritance during
212 cytokinesis. Unlike control parasites, which display individual, segmented apicoplasts in
213 daughter parasites, PfAnchor-deficient parasites retained a single, interconnected
214 apicoplast linking multiple daughter parasites (**Figure 4b, c**). Live microscopy previously
215 revealed a subset of daughter parasites lacking apicoplast signal, and U-ExM further
216 confirmed this phenotype, showing that these apicoplast-negative merozoites had
217 separated from the cluster and moved freely (**Figure 4d**). This resulted in two distinct
218 populations of daughter parasites in the PfAnchor-deficient samples: (1) parasites
219 connected by a shared apicoplast traversing the basal complex (**Figure 4e**), and (2) parasites
220 that were physically separated from the residual body but devoid of apicoplast signal (**Figure**
221 **4d**). Notably, while PfAnchor-deficient parasites displayed severe apicoplast inheritance
222 defects, mitochondria biogenesis and division remained unaffected, with each daughter cell

223 inheriting a single mitochondrion (**Figure S7**). These findings establish PfAnchor as a critical
224 factor of apicoplast division and inheritance, and its loss likely prevents parasite propagation
225 and survival.

226 To further investigate the impact of Anchor depletion on apicoplast structure, we
227 performed cryo-focused ion beam (cryo-FIB) milling and cryo-electron tomography (cryo-
228 ET) on PfAnchor iKD parasites in the presence and absence of aTC. To ensure stage-matched
229 analysis, we treated cultures with Compound 1 (4-[2-(4-fluorophenyl)-5(1-methylpiperidine-
230 4-yl)-1H-pyrrol-3-yl]pyridine or C1), a reversible protein kinase G inhibitor that arrests
231 schizonts immediately prior to egress by preventing parasitophorous vacuole membrane
232 (PVM) rupture [46, 50]. C1-stalled schizonts were Percoll-purified and incubated in media
233 containing 2.5 μM C1 for 2–3 hours before fixation. We analyzed a total of 12 tomograms from
234 PfAnchor-expressing (+aTC) parasites, all containing identifiable apicoplasts, and 9
235 tomograms from PfAnchor-deficient (–aTC) parasites that featured apicoplasts. The
236 apicoplast was distinguished in tomograms based on its characteristic four-membrane
237 structure. 2D Measurement of the smallest internal diameter, taken from a 2D slice at the
238 center of the apicoplast volume, revealed no significant difference between PfAnchor-
239 expressing and PfAnchor-deficient parasites (**Figure S8a**). In both PfAnchor-expressing and
240 PfAnchor-deficient parasites, we observed cryo-EM densities within the intermembrane
241 space of the apicoplast (**Figure 4f**). These densities included dense intermembrane buds,
242 defined as electron-dense tethering structures between neighboring apicoplast membranes
243 (**Figure 4f, blue arrows**). Interestingly, the frequency of these dense intermembrane buds
244 was significantly reduced in PfAnchor-deficient parasites, with PfAnchor-expressing
245 parasites present ~2.2 dense buds per apicoplast on average (S.D. = 1.2), while PfAnchor-
246 deficient parasites averaged ~1.1 dense buds per apicoplast (S.D. = 1.2).

247 In addition to the dense intermembrane buds, we identified enclosed membrane-like
248 buds—small, circular densities forming between apicoplast membranes (**Figure 4f, green**
249 **arrows**). Unlike the dense intermembrane buds, the number of enclosed buds remained
250 unchanged between PfAnchor-expressing and PfAnchor-deficient parasites. This suggests
251 that while PfAnchor influences the formation or maintenance of dense intermembrane

252 buds, it does not significantly impact the presence of enclosed buds, indicating that some
253 aspects of membrane organization remain intact. Beyond these structures, we observed
254 additional internal features within the apicoplast lumen. These included single-layer and
255 double-layer membrane structures, which may represent distinct internal compartments or
256 intermediates in apicoplast remodeling (**Figure S8b-e**). Quantification of single-layer
257 membrane structures revealed no significant differences in their abundance or internal
258 diameter between PfAnchor-expressing and PfAnchor-deficient parasites (**Figure S8c, d**),
259 suggesting that their formation is independent of PfAnchor. However, double-layer
260 membrane structures were exclusively detected in PfAnchor-deficient parasites (**Figure**
261 **S8e**), raising the possibility that PfAnchor depletion alters the internal architecture of the
262 apicoplast. These findings suggest that while PfAnchor is not required for overall membrane
263 biogenesis, it may play a role in maintaining the organization or remodeling of apicoplast
264 membrane organization, potentially influencing its division and inheritance.

265 **Loss of apicoplast-branched structure rescues growth in PfAnchor-deficient parasites.**

266 We hypothesized that the egress defects observed in PfAnchor-deficient parasites
267 result from physical tethering of daughter merozoites by the branched apicoplast structure
268 and that disrupting this tethering could restore parasite viability. Bacterial translation
269 inhibitors such as doxycycline, clindamycin, and azithromycin are known to disrupt
270 apicoplast structure, leading to the formation of apicoplast-like vesicles during the second
271 cycle of treatment and parasite death [13, 45]. The growth of parasites treated with bacterial
272 translation inhibitors can be rescued with the addition of exogenous IPP [13], leading to
273 parasites growing with apicoplast-like vesicles instead of a branching apicoplast and
274 irreversible loss of the apicoplast genome [51]. The high cost and the difficulties associated
275 with the IPP-rescue system [13] for long-term studies led to the development of an
276 apicoplast bypass system by Swift et al. in 2020 [45]. This system introduces four enzymes
277 into the cytoplasm of the parasite, allowing for IPP synthesis via the mevalonate (MVA)
278 pathway in the cytoplasm, thereby bypassing the endogenous methylerythritol phosphate
279 (MEP) pathway in the apicoplast. By adding mevalonate to the growth medium, the bypass

280 system significantly reduces the cost and improves the feasibility of long-term experimental
281 studies.

282 To test our hypothesis, we used the apicoplast bypass PfAnchor^{Mev} iKD cell line and
283 treated parasites with the antibiotic azithromycin (AZ) to prevent apicoplast branching
284 during PfAnchor knockdown [13, 52]. Briefly, PfAnchor^{Mev} iKD parasites were initially cultured
285 in the presence of 50 µM mevalonate (Mev) and 100 nM AZ for 7 days. The parasites were
286 then split into four experimental groups: (1) +aTC -Mev (green), (2) -aTC -Mev (orange), (3)
287 +aTC +Mev (blue), and (4) -aTC +Mev (red) (**Figure 5a**). These groups were cultured for an
288 additional 8 days, taking samples every 2 days for growth analysis. To prevent culture
289 collapse, parasite cultures were diluted (1:8) every 2 days. U-ExM validated the loss of the
290 apicoplast branching structure and PCR analysis confirmed the loss of the apicoplast
291 genome regardless of the presence of PfAnchor (**Figure 5c, g, Figure S9**).

292 Growth analysis revealed distinct phenotypes depending on PfAnchor expression
293 and the presence of Mev. In parasites with apicoplast-like vesicles (+AZ), parasites
294 supplemented with Mev displayed equivalent growth rates regardless of PfAnchor
295 expression (**blue and red lines overlapping, Figure 5b**), indicating that disruption of the
296 branched apicoplast structure fully rescued the growth defects associated with PfAnchor
297 depletion. Conversely, parasites with apicoplast-like vesicles but not supplemented with
298 Mev failed to grow regardless of PfAnchor expression (**green and orange lines overlapping,**
299 **Figure 5b**), validating the experimental setup. These results demonstrate that the loss of the
300 branched apicoplast structure is sufficient to fully rescue the growth defects in PfAnchor-
301 deficient parasites. This finding underscores the critical role of PfAnchor in apicoplast
302 fission. Since parasite viability is restored in the absence of a branched apicoplast, it
303 appears unlikely that PfAnchor has any other essential functions beyond facilitating
304 apicoplast fission.

305 As controls we tested the growth of parasites with a branched apicoplast (-AZ) in the
306 presence or absence of Mev or PfAnchor. Branched apicoplast PfAnchor-expressing
307 parasites showed robust growth with or without Mev supplementation (**green and blue lines**

308 **overlapping, Figure S10**). Branched apicoplast PfAnchor-deficient parasites failed to grow
309 without Mev, as evidenced by a decline in parasitemia (**orange line, Figure S10b**).
310 Interestingly, PfAnchor-deficient parasites supplemented with Mev initially exhibited
311 reduced growth but subsequently recovered, achieving growth rates comparable to
312 PfAnchor-expressing parasites (**red line, Figure S10b**). We hypothesize that this initial
313 recovery of growth is caused by free merozoites which contain no apicoplast in the PfAnchor
314 population (**Figures 3d, 4b**) that can survive and propagate when supplemented with Mev.

315

316 **Apicoplast-like vesicles are retained in daughter parasites in association with**
317 **mitochondria, independent of PfAnchor.**

318 To investigate the fate of the apicoplast following its disruption by azithromycin, we
319 examined the spatial organization and inheritance of the resulting apicoplast-like vesicles
320 using U-ExM (**Figure 5c, g**). In PfAnchor-expressing parasites, the majority of apicoplast-like
321 vesicles were excluded from the daughter parasites and instead localized within the residual
322 body at the completion of cytokinesis (**Figure S11**). However, a subset of apicoplast-like
323 vesicles remained within daughter cells, and these retained vesicles were consistently
324 associated with the mitochondrion (**Figure 5c, S11**). This suggests that mitochondrial
325 association plays a key role in apicoplast vesicle inheritance, while vesicles not tethered to
326 the mitochondrion are largely excluded from daughter parasites during cytokinesis.

327 To determine whether PfAnchor is required for apicoplast-like vesicle inheritance, we
328 examined PfAnchor-deficient parasites and found that their vesicle localization and
329 distribution were largely similar to PfAnchor-expressing parasites (**Figure 5g, S12**). However,
330 quantification revealed a modest but significant increase in the number of mitochondrion-
331 associated apicoplast vesicles in PfAnchor-deficient parasites compared to PfAnchor-
332 expressing parasites (**Figure 5e**). This suggests that while PfAnchor is not required for vesicle
333 retention, its depletion may subtly influence the balance between vesicle inheritance and
334 clearance. Despite this increase, the spatial distribution of apicoplast-like vesicles along the
335 mitochondrion was unchanged between conditions (**Figure 5f**), reinforcing the conclusion

336 that PfAnchor does not impact the positioning of retained vesicles. As the mitochondrion
337 served as a spatial reference for apicoplast vesicle distribution, we quantified mitochondrial
338 length to ensure that mitochondrial organization remained unchanged in the presence or
339 absence of PfAnchor. No significant differences in mitochondrial length were observed
340 between PfAnchor-expressing and PfAnchor-deficient parasites following azithromycin
341 treatment (**Figure 5d**), confirming that any differences in apicoplast-like vesicle localization
342 would not be due to changes in mitochondrial morphology. Together, these data indicate that
343 mitochondrial association is a key determinant of apicoplast vesicle retention, while
344 PfAnchor is not required for their inheritance.

345 **PfAnchor interacts with PfDyn2 to facilitate apicoplast fission.**

346 Knockdown of PfAnchor disrupts apicoplast segregation and positioning, yet its
347 precise molecular function remains unclear. To identify potential interacting partners, we
348 performed immunoprecipitation (IP) experiments using two PfAnchor-tagged cell lines
349 (PfAnchor iKD and PfAnchor^{Mev} iKD), followed by unbiased mass spectrometry. Parental
350 untagged (3D7-Cas9) parasites served as a control to distinguish specific interactors from
351 background proteins. Principal component analysis (PCA) of the mass spectrometry data
352 confirmed the specificity of PfAnchor-associated interactions, as PfAnchor clustered
353 distinctly from background interactors (**Figure 6a, Supp Data 2**). Among the most highly
354 enriched proteins, PfDyn2 emerged as a primary interactor, supporting its role as a key
355 regulator of apicoplast and mitochondrial fission [23, 24]. In addition to PfDyn2, PCA
356 identified PfHsp70 (PF3D7_0818900) as a secondary interactor, suggesting a possible role
357 in stabilizing protein complexes during apicoplast division [53, 54]. Beyond the PCA analysis,
358 PfAnchor pulldown experiments identified additional interactors uniquely present in the
359 PfAnchor dataset (**Figure 6c**). Among these, PfActin1 was specifically enriched, consistent
360 with its established role in cytoskeletal regulation of organelle segregation [47, 55]. PfCinch,
361 a basal complex protein [56], was also identified, suggesting a possible link between
362 PfAnchor and cytoskeletal structures involved in organelle positioning. These findings
363 provide strong evidence that PfAnchor interacts with PfDyn2, reinforcing its involvement in
364 apicoplast fission. The identification of PfHsp70 as a secondary interactor suggests a

365 potential chaperone function that may contribute to the stability of the fission complex.
366 Additionally, the enrichment of PfActin1 and PfCinch supports a possible cytoskeletal role
367 in apicoplast segregation.

368 To complement our IP approach and further define the PfAnchor interactome, we
369 performed proximity-dependent biotin labeling (BioID), followed by mass spectrometry.
370 BioID enables the identification of proteins in close spatial proximity to PfAnchor, including
371 transient or membrane-associated interactors. Two independent biological replicates of
372 BioID with PfAnchor-BirA-HA(**Figure S13**) were performed, with parental untagged parasites
373 serving as a control to account for background labeling. PCA analysis of BioID mass
374 spectrometry data demonstrated that PfAnchor clustered distinctly from background
375 interactors, with PfDyn2 emerging as the most enriched protein in proximity to PfAnchor
376 (**Figure 6b, Supp Data 3**). This further supports a functional association between PfAnchor
377 and PfDyn2, consistent with the results of our immunoprecipitation experiments. Additional
378 proteins detected in the BioID dataset included components of the MCM complex, though
379 their potential relevance to apicoplast function remains unclear. PfDyn2 was consistently
380 enriched in both BioID and IP datasets, reinforcing its role as PfAnchor's primary interactor
381 (**Figure 6d**). This strong association suggests that PfAnchor may act as an adaptor or
382 regulator in apicoplast fission, potentially recruiting PfDyn2 to the organelle membrane.
383 Together, these findings support a model in which PfAnchor serves as a key adaptor protein,
384 bridging cytoskeletal and membrane remodeling factors to facilitate apicoplast fission
385 (**Figure 6e**).

386

387 **Discussion**

388 This study reveals a fundamentally new mechanism of parasite death and identifies
389 PfAnchor as an essential adaptor that enables apicoplast fission in *Plasmodium falciparum*.
390 We show that PfAnchor localizes to the apicoplast throughout the intraerythrocytic cycle
391 and is required for its division and inheritance. Conditional depletion of PfAnchor disrupts
392 apicoplast fission, resulting in physically tethered merozoites that fail to complete

393 cytokinesis and cannot invade new red blood cells. This phenotype demonstrates, for the
394 first time, that failure to divide the apicoplast can directly impair cell division and lead to
395 same-cycle parasite death. Additionally, we highlight the potential of targeting apicoplast
396 morphology as a novel strategy for inducing same-cycle parasite death, positioning
397 PfAnchor as a promising therapeutic target for malaria intervention.

398

399 **PfAnchor's Structural Features and Functional Implications**

400 Alphafold3 predictions and domain analysis suggest that PfAnchor contains a
401 pleckstrin homology (PH) domain, a common motif for membrane binding. Given that the
402 apicoplast membrane is enriched in PI3P [57, 58], it is plausible that PfAnchor's PH domain
403 mediates its localization. Additionally, PfAnchor's N-terminal region contains a hydrophobic
404 helix, which carries a mutation linked to resistance against actin-polymerization inhibitors
405 [59]. The co-occurrence of mutations in PfAnchor and profilin (a key actin regulator) in
406 parasites resistant to MMV020291, an antimalarial that targets actin polymerization,
407 suggests a functional link between PfAnchor and actin dynamics [59]. Actin dynamics are
408 increasingly recognized as important for apicoplast segregation, and our identification of
409 PfActin1 as a PfAnchor interactor supports this idea [47, 55]. In other eukaryotic systems,
410 profilin-actin interactions regulate fission events by remodeling membrane-associated
411 cytoskeletal networks [60-62]. By analogy, PfAnchor may facilitate actin polymerization at
412 the apicoplast fission site, potentially through indirect interactions with profilin. Future
413 studies should investigate whether targeted disruption of PfAnchor's hydrophobic helix
414 affects actin-mediated apicoplast segregation.

415

416 **PfAnchor's Role in Organelle Structure and Function**

417 Despite its role in apicoplast fission, PfAnchor is not required for overall apicoplast
418 biogenesis. Parasites lacking PfAnchor remain viable when the metabolic function of the
419 apicoplast is bypassed using mevalonate supplementation. Furthermore, treatment with

azithromycin, which eliminates the branched apicoplast structure, rescued the growth defects of PfAnchor-deficient parasites. These findings confirm that PfAnchor's primary function is in organelle fission rather than metabolism. Interestingly, while PfAnchor is not required for other apicoplast functions such as fatty acid synthesis, iron-sulfur cluster biosynthesis, or heme production, its potential role in isoprenoid precursor synthesis remains unclear. Inhibition of the MEP pathway using fosmidomycin results in an unbranched, stagnant apicoplast [13, 14]; however, PfAnchor-deficient parasites still exhibit normal biogenesis and branching, making a direct role in isoprenoid metabolism unlikely.

Cryo-electron tomography of PfAnchor-deficient and control parasites further revealed the presence of distinct electron-dense structures within the apicoplast. We identified two main morphologies: "dense buds," small, localized densities between membranes, and "enclosed buds," larger invaginated membrane profiles. Similar membranous profiles—sometimes described as tubular whorls—have been reported in apicoplasts of *Plasmodium* and *Toxoplasma*, though their functional role remains unresolved [63-65]. Comparative plastid systems such as etioplasts, also contain analogous intra-organelle structures, including protein complexes, plastoglobuli, and tubular arrays involved in membrane remodeling and metabolic scaffolding [66]. The persistence of these features in the *Plasmodium* apicoplast, independent of PfAnchor expression, raises intriguing questions about their function in membrane remodeling, metabolite transport, or structural maintenance of the apicoplast's four-membrane architecture. Whether these intramembrane structures persist within the apicoplast-like vesicles remains an open question. Further investigation will be required to determine whether these features are involved in apicoplast homeostasis, division, or are vestiges of its photosynthetic ancestry.

Mitochondrion-Apicoplast Tethers and Organelle Inheritance

Our findings provide the first high-resolution evidence that mitochondrion-associated apicoplast-like vesicles are selectively inherited [67], reinforcing the functional

448 dependency between these organelles [49, 65]. While most vesicles were excluded from
449 daughter cells, the retained subset consistently colocalized with mitochondria (**Figures 5,**
450 **S10, S11**). This strong spatial association suggests a role for physical tethering between the
451 apicoplast and mitochondrion in ensuring faithful organelle inheritance. Moreover, the
452 molecular components mediating this tethering are likely preserved on apicoplast-like
453 vesicles that are inherited. Consistent with this idea, electron-dense structures at the
454 interface between the mitochondrion and apicoplast have recently been described by cryo-
455 ET in *P. falciparum*, suggesting the presence of defined tethering complexes at points of
456 close membrane contact [65]. While we did not specifically image vesicles in contact with
457 mitochondria by cryo-ET in this study, it remains an open and important question whether
458 these dense tethering structures persist in the apicoplast-like vesicles that are inherited
459 following AZ treatment. Interestingly, PfAnchor depletion resulted in a slight but significant
460 increase in mitochondrion-associated vesicles (**Figure 5e**), indicating that while PfAnchor is
461 not required for inheritance, its loss may alter the balance between vesicle retention and
462 clearance. The nature of the mitochondrion–apicoplast tethers remains to be elucidated,
463 but it is likely mediated by tethers that help coordinate spatial organization during division.
464 Are these tethers simple structural linkages, or true membrane contact sites that enable
465 metabolite exchange or signaling? The role of the cytoskeleton, particularly actin, in
466 stabilizing these tethers warrants further investigation, as cytoskeletal elements are known
467 to contribute to apicoplast segregation in *Plasmodium* and other apicomplexans[47, 55].

468

469 **PfAnchor Interacts with PfDyn2 and the Cytoskeleton**

470 To elucidate the molecular function of PfAnchor, we performed immunoprecipitation
471 and proximity labeling experiments, which identified PfDyn2 as its primary interacting
472 partner. PfDyn2 is a dynamin-related GTPase known to mediate apicoplast and
473 mitochondrial fission [23, 24]. The enrichment of PfDyn2 in both datasets supports a model
474 in which PfAnchor functions as a dynamin adaptor, likely recruiting PfDyn2 to the apicoplast
475 membrane to facilitate membrane fission. This is analogous to mitochondrial fission

476 adaptors in other eukaryotes, which tether dynamin-related proteins to fission sites.
477 Additionally, we identified interactions between PfAnchor and cytoskeletal components,
478 including PfActin1 and PfCINCH, suggesting a potential role in coordinating apicoplast
479 fission with parasite cytoskeletal dynamics [55, 56]. Notably, the basal complex, which
480 facilitates cytokinesis, may also coordinate organelle fission. Positioned at the parasite
481 plasma membrane, it could serve as a platform for synchronizing apicoplast and
482 mitochondrial division with daughter cell separation. Future studies should examine
483 whether basal complex components, such as PfCINCH, actively remodel membranes or
484 anchor fission machinery at the apicoplast and mitochondria during schizogony.
485 Additionally, PfHsp70 (PF3D7_0818900), identified in our interactome analysis, could
486 stabilize the fission complex, as its homologs in other eukaryotes support mitochondrial and
487 chloroplast division by assisting in protein complex assembly and function [54, 68].

488 Finally, we identified PfAnchor via proximal labeling using PfMCMBP, a DNA helicase
489 that functions during DNA replication [39]. While reciprocal proximity labeling with PfAnchor
490 as bait confirmed the presence of PfMCMBP and PfMCM5, our immunoprecipitation
491 experiments did not recover these proteins, suggesting that they are not direct binding
492 partners of PfAnchor. Instead, their detection in proximity labeling assays likely reflects their
493 spatial localization within the parasite during schizogony rather than a functional interaction.
494 The apicoplast and PfAnchor are positioned near the centriolar plaque (CP) immediately
495 before segmentation (**Figure S6**), and the CP is surrounded by nuclear pore complexes,
496 indicating active nucleocytoplasmic transport in this region [69]. Given this, it is plausible
497 that the MCM complex, which shuttles between the cytoplasm and nucleus during DNA
498 replication, transiently occupies a similar cellular space. While a direct functional
499 relationship between PfAnchor and the MCM complex remains unlikely, these findings
500 highlight the complex organization of cellular structures during *P. falciparum* blood-stage
501 parasites replication and underscore the utility of proximity labeling in capturing transiently
502 colocalized proteins within the parasite.

503

504 **PfAnchor in Other Developmental Stages**

505 Although our study establishes PfAnchor's role in blood-stage parasites, its
506 expression in other life cycle stages suggests broader functions. Transcriptomic data
507 indicate that PfAnchor is expressed during gametocytogenesis, where male and female
508 gametocytes harbor a single, non-branching apicoplast [70, 71]. Whether PfAnchor plays a
509 role in gametocyte development or is dispensable at this stage remains unclear. By contrast,
510 during mosquito and liver stages, parasites undergo extensive replication, and their
511 apicoplasts adopt a branching tubular morphology similar to blood stages [72]. This implies
512 that apicoplast fission must occur to ensure organelle inheritance during liver merozoite and
513 sporozoite formation. Investigating PfAnchor's function in these stages could reveal
514 conserved mechanisms of apicoplast division throughout the parasite life cycle and identify
515 new transmission-blocking targets.

516 Our findings identify PfAnchor as an essential adaptor linking dynamin-mediated
517 membrane scission to actin-dependent apicoplast partitioning. In many eukaryotes, the
518 same dynamin-related protein (such as Yeast Dnm1 or Human Drp1) is recruited to different
519 organelles via organelle-specific adaptors, enabling functional specificity despite shared
520 GTPase machinery [25, 26]. Similarly, in *Plasmodium*, the dynamin-related protein Dyn2
521 mediates fission of both the mitochondrion and the apicoplast (PMID: 39611847). Here, we
522 demonstrate that PfAnchor is specifically required for apicoplast division but dispensable
523 for mitochondrial fission, revealing the first known organelle-specific adaptor for dynamin
524 function in this system. The adaptor responsible for mitochondrial fission in *Plasmodium*
525 remains to be identified. The selective requirement for PfAnchor in apicoplast division may
526 reflect the evolutionary origin and complex membrane architecture of this organelle, which
527 is derived from a red algal endosymbiont and surrounded by four membranes. Importantly,
528 studying *Plasmodium* and other myxozoans—including dinoflagellates—offers a unique
529 opportunity to explore how a single dynamin pathway is adapted to remodel and divide
530 organelles of diverse evolutionary origins within the same cellular environment. While the
531 apicoplast in Apicomplexa has evolved into a non-photosynthetic, metabolism-focused
532 organelle essential for parasitism, dinoflagellates retain photosynthetic plastids derived
533 from the same secondary endosymbiotic event. This divergence provides a powerful

534 comparative framework to dissect how conserved membrane fission machinery is
535 repurposed across lineages to accommodate organelle-specific architectures and
536 functions. Given that apicoplast division is essential for parasite survival and lacks a
537 counterpart in human cells, targeting PfAnchor or its associated machinery could offer a
538 promising new avenue for antimalarial strategies. Future studies will be critical to uncover
539 the molecular composition and regulation of this fission pathway and to understand how
540 cytoskeletal remodeling and membrane scission are coordinated to ensure faithful
541 inheritance of the apicoplast.

542

543 **Materials and Methods**

544 **Parasite culture:**

545 The 3D7 *Plasmodium falciparum* strain, obtained from the Walter and Eliza Hall
546 Institute (Melbourne, Australia) was cultured in human O^+ RBCs at 4% hematocrit in RPMI-
547 1640 containing 25 mM HEPES, 50 mg/L hypoxanthine, 0.21% sodium bicarbonate, and
548 0.5% w/v Albumax II [73]. Cultures were incubated at 37 °C while shaking in a gas mixture of
549 1% O_2, 5% CO_2, and 94% N_2 as previously described The PfAnchor iKD (smV5-Tet
550 Pf3D7_0613600) and PfAnchor^{Mev} iKD (smV5-Tet Pf3D7_0613600 in PfMev background) cell
551 lines were maintained under selection of 2.5 nM WR99210 and supplemented with 500 nM
552 anhydrotetracycline (aTC).

553 **Plasmid generation and transfection:**

554 To generate the PfMCMBP-BirA-HA cell line for proximal labeling, the homology region
555 of pSAB60 (PfMCMBP-3HADD [39]) was cut with Not1/Xho1 and cloned into our BirA plasmid
556 (pRR28) [74] to create pSAB99. To generate the PfMCMBP-BirA-HA strain, 100 µg of pSAB99
557 plasmid was transfected into synchronized ring staged parasites using electroporation.
558 Upon transfection, stable single crossover parasites were selected by cycling 2.5 nM
559 WR99210 on and off as previously described [75]. Integration of pSAB99 plasmid into the

560 genome of 3D7 was confirmed via PCR using primer pairs oSAB504/oJDD44,
561 oSAB505/oJDD44, and oSAB504/oSAB506 **(Figure S1**).

562 To create the Pf3D7_0613600-smV5-Tet (PfAnchor iKD) plasmid, the Pf3D7_0613600
563 5' and 3' homology regions were PCR amplified from 3D7 genomic DNA with
564 oligonucleotides oJDD4308/4310 and oJDD4307/4309 respectively. The two pieces were
565 fused together using Sequence Overlap Extension PCR (SOE-PCR) using oJDD4803/4309
566 and the piece was digested using Not1/Nco1 and ligated onto pRR92 [56] (which contains
567 the smV5 epitope tag, ten copies of the Tet-aptamer for the TetR-DOZI aptamer knockdown
568 system, and the expression cassette for human dihydrofolate reductase (hDHFR)) to form
569 pSAB177. To create Pf3D7_0613600 targeting guide RNA plasmid, oJDD4347/4348 were
570 annealed, phosphorylated, and ligated into BpiI-digested pRR216 [23] to generate pSAB175.
571 All oligonucleotide sequences are shown in **Table S1**. To generate the PfAnchor iKD strain,
572 100 µg of pSAB177 plasmid was linearized with Stu1 and transfected into 3D7-Cas9
573 parasites, along with 100 µg of pSAB175 and supplemented with 500 nM aTC. 24 hours
574 following transfection parasites were treated with 5 nM WR99210 for 7 days before
575 maintaining on 2.5 nM WR99210 and 500 nM aTC until resistant parasites were detected.
576 Integration of pSAB177 plasmid into the genome of 3D7 was confirmed via PCR using primer
577 pairs oSAB243/oJDD2933, oSAB367/oSAB2933, oSAB243/oSAB366, and
578 oSAB367/oSAB366. Primer binding locations and predicted PCR product sizes are listed in
579 **Figure S4a-b**.

580 To generate the PfAnchor^{Mev} iKD strain, 350 µL of RBCs were electroporated using the
581 GenePulser XCell system (Bio-Rad) with 75 µg each of pSAB175 and linearized pSAB177
582 obtained by digestion with EcoRV. The electroporated RBCs were combined with 1 mL
583 of PfMev^{attB} parasite culture at 3% parasitemia and cultured in 10 mL of CMA (Complete
584 Medium with Albumax) for two days. Subsequently, the cultures were transferred to selective
585 medium containing 2.5 nM WR99210 for seven days. Afterward, the cultures were returned
586 to CMA until parasites were detected on blood smears, at which point WR99210 was
587 reintroduced to the medium. The transgenic parasite culture was cloned by limiting dilution.
588 Clones were screened for an intact aptamer array via PCR amplification using primers

589 oSAB249 and oJDD44. Clone F3 was selected for further experiments (**Figure S14**).
590 Integration of pSAB177 plasmid into the genome of NF54-PfMev parasites [45] was
591 confirmed via PCR using primer pairs oSAB243/oJDD2933, oSAB367/oSAB2933,
592 oSAB243/oSAB366, and oSAB367/oSAB366. Primer binding locations and predicted PCR
593 product size found in **Figure S4a, c**.

594 To generate the PfAnchor-BirA-HA proximal labeling plasmid, homology region from
595 pSAB177 was amplified using oSAB356/358 and the piece was digested using Not1/Xho1
596 and ligated into pSAB99 to create pSAB233. To generate the PfAnchor-BirA-HA strain, 100 µg
597 of pSAB233 plasmid was linearized with Stu1 and transfected into 3D7-Cas9, along with 100
598 µg of pSAB175. 24 hours following transfection parasites were treated with 5 nM WR99210
599 for 7 days before maintaining on 2.5 nM WR99210 until resistant parasites were detected.
600 Integration of pSAB233 plasmid into the genome of 3D7 was confirmed via PCR using primer
601 pairs oSAB243/oJDD44, oSAB243/oSAB366, oSAB367/oJDD44, and oSAB367/oSAB366.
602 Primer binding locations and predicted PCR product size found in **Figure S13**. All parasite
603 lines used in this study are listed in **Table S2**.

604 **Growth analysis:**

605 For parasite growth analysis, parasite cultures were synchronized at the schizont
606 stage by either density centrifugation using 60% Percoll PLUS or by magnetic separation
607 using MACs columns, incubated at 37 °C for 2-3 hours with fresh erythrocytes, and then
608 newly invaded ring stage parasites were purified by treatment with 5% w/v sorbitol. In three
609 biological replicates, cultures were plated and incubated at 37 °C at 4% hematocrit in the
610 presence or absence of aTC. Over the course of 96 hours (2 intraerythrocytic cycles)
611 timepoints were taken at 0, 48, and 96 hours and the parasitemia was determined by
612 counting a minimum of 400 RBCs.

613 **Sodium carbonate extraction:**

614 For the sodium carbonate extraction assay, the protocol from Liffner *et al* was used
615 [76]. Saponin-lysed parasite pellets from 10 mL of high parasitemia late schizonts (40-48 hpi)
616 were resuspended in 100 µL of Milli-Q water and snap-frozen using liquid nitrogen four times

617 before passing through a 28 gauge needle. Samples were centrifuged for 10 minutes at
618 18,000 x g at 4 °C, with the supernatant reserved as the hypotonic (water soluble) sample.
619 The pellet was washed twice with 500 µL Milli-Q water and once with 500 µL 1x PBS before
620 the pellet was resuspended in 100 µL 0.1 M sodium carbonate (Na_2CO_3) and incubated in ice
621 for 30 minutes. The sample was centrifuged at 18,000 x g at 4 °C for 5 minutes and the
622 supernatant was reserved as the sodium carbonate (peripheral membrane) sample. The
623 remaining pellet was washed 3 times in 100 µL 1x PBS before resuspending the pellet in 100
624 µL ice cold 0.1% Triton X-100/PBS and incubated for 30 minutes on ice. Samples were
625 centrifuged at 18,000 x g at 4 °C and the supernatant was reserved before the pellet was
626 washed and resuspended in 100 µL 1x PBS. Samples were analyzed by western blotting.

627 **Proteinase K protection:**

628 For Proteinase K protection assay, the protocol from Liffner *et al* was used [76]. 3x 10
629 mL cultures of schizonts (36-48 hpi) were lysed with 0.15% saponin/PBS-protease inhibitors
630 (Sigma S8820-20 TAB, 1 tab for 100 mL PBS) for 10 minutes before centrifuging at 18,000 x g
631 for 10 minutes at 4 °C. Pellets were washed 3x in 1x PBS-protease inhibitors before further
632 treatment. Three treatments were performed: one tube treated with 250 µL SOTE buffer (0.6
633 M Sorbitol, 20 mM Tris HCl, 2 mM EDTA) alone. A second tube was treated with 250 µL 0.02%
634 w/v digitonin in SOTE for 10 minutes on ice before centrifuging at 800 x g for 10 minutes at 4
635 °C. The resulting pellet was washed once with SOTE buffer. A third tube of sample was
636 treated with digitonin followed by treatment with 0.1 mg/mL Proteinase K in SOTE for 30
637 minutes on ice. The sample was then centrifuged at 18,000 x g for 10 minutes at 4 °C before
638 inactivating the Proteinase K by treatment of the pellet with 100 µL of 5 mM PMSF
639 (ThermoFisher #36978) in SOTE buffer for 10 minutes on ice. Samples were analyzed by
640 western blotting.

641 **Western Blot:**

642 Protein samples were collected by saponin lysis with 0.15% w/v saponin/PBS-
643 protease inhibitors for 10 minutes on ice, parasite material was pelleted by centrifugation
644 before washing 3x with PBS-protease inhibitors. Parasite pellets were resuspended in

645 Laemmli sample buffer + 5% v/v β-mercaptoethanol (Aldrich), heated at 37 °C for 1 hour with
646 vortexing every 30 minutes, and separated by size using BioRad 4-20% Mini-PROTEAN TGX
647 stain free gels (BioRad Cat. #4568095) at 200 V for 40 minutes. Proteins were transferred to
648 a nitrocellulose membrane using a BioRad Transblot Turbo Transfer System with the
649 MixedMW setting (25 V, 1.3 A, 7 minutes) before blocking using 1:5 BioRad EveryBlot Blocking
650 Buffer (BioRad Cat. #12010020): PBS for 30 minutes at room temperature. Membranes were
651 incubated in primary antibodies (listed in Table S3) overnight at 4 °C, washed 3x in 1x TBS+
652 0.01% Tween20 before incubating with secondary antibodies (listed in Table S3) at room
653 temperature for 45 minutes. Western Blots were visualized using a BioRad ChemiDocMP
654 Imaging system. Western blot quantification was done using BioRad Image Lab V6.1
655 software.

656 **Live microscopy:**

657 Glass bottomed microscopy dishes (Cellvis D35-20-1.5-N) were coated with 0.5
658 mg/mL concanavalin A (Sigma, C0412-5MG) solution for 1 hour at 37 °C before 3x washes
659 with Milli-Q water. Synchronous late stage +aTC or -aTC parasites were purified by MACs
660 columns and treated with compound 1 [46] before being applied to the glass bottomed
661 dishes and incubated for 3 hours at 37 °C to allow parasites to adhere. After 3 hours samples
662 were washed with 1 mL complete phenol-red-free RPMI. Brightfield and fluorescent images
663 were taken every 0.5-4.5 seconds for 30 minutes per sample using a Leica DMI6000 B
664 microscope and a 63x objective with a numerical aperture of 1.4.

665 **Ultrastructure Expansion Microscopy (U-ExM) :**

666 12 mm round coverslips (Fisher, Cat# NC1129240) were treated with poly-D-lysine for
667 1 hour at 37 °C, washed twice with MilliQ water, and placed in the wells of a 24 well plate.
668 Five hundred uL of parasite cultures adjusted to roughly 1% hematocrit was added to the
669 wells containing a coverslip. Samples were allowed to settle for 30 minutes at 37 °C before
670 culture supernatant was removed and 500 µL of 4% v/v PFA in 1x PBS was gently added along
671 the side of the well and incubated at 37 °C for 20 minutes. Coverslips were washed once with
672 1x PBS before being treated with 500 µL of 1.4% v/v formaldehyde/2% v/v acrylamide (FA/AA)

673 in PBS overnight at 37 °C. Gelation, denaturation, staining, and expansion of gels were
674 performed as previously described [21]. Stained gels were imaged using a Zeiss LSM900
675 AxioObserver with an Airyscan 2 detector. Images were taken using a 63x Plan-Apochromat
676 objective lens with a numerical aperture of 1.4. All antibodies and their dilutions used in
677 this study are listed in **Table S3**.

678 **Cryo-Electron Tomography**

679 ***Sample preparation***

680 PfAnchor iKD parasites were grown and synchronized as described above. Late
681 schizont pellets were obtained via percoll purification and allowed to incubate in 5 mL of
682 media with 2.5 uM Compound 1 [46] for 3 hours. Parasites were chemically fixed with 4%
683 PFA/0.01% glutaraldehyde for 20 minutes before resuspending in PBS prior to cryo-electron
684 tomography.

685 ***Cell vitrification:***

686 Quantifoil Cu R2/1 grids were glow-discharged for 1 minute at 25 mA using an
687 EmiTech K100X glow discharger (EMS). 4 µL of PfAnchor iKD *Compound 1 arrested* parasites
688 grew in presence or absence of aTC (previously fixed with 4% PFA/glutamate PBS solution)
689 cell culture were applied in 4 µL to each grid, manually back-blotted on one side (22°C and
690 100% humidity) for 3-4 seconds, and plunge-frozen in a 1:1 mixture of liquid ethane and
691 propane using a Vitrobot Mk IV (ThermoFisher). Plunge-frozen grids were stored in liquid
692 nitrogen.

693 ***Cryo-FIB Milling:***

694 Cryo-FIB milling was performed using an Aquilos 2, a cryo-dedicated DualBeam
695 microscope (ThermoFisher). Cryo-grids were sputter coated for 10 seconds, followed by a
696 layer of organic platinum deposited by the gas injection system for 15 seconds, followed by
697 another 10 seconds of sputter coating. Cell clusters were milled to generate lamella at ~150-
698 200 nm thickness, using 0.1-0.3 nA ion beam current for rough milling and 30-50 pA for final
699 polishing.

700 ***Cryo-ET:***

701 Cryo-FIB milled lamella grids were transferred to a Titan Krios 3Gi microscope
702 (ThermoFisher, FEI), equipped with a 300 kV field emission gun, a Selectris energy filter and
703 Falcon 4i direct electron detector. Tilt series were collected using Tomo5 software
704 (ThermoFisher) at 42,000x magnification (2.9 Å pixel size) and the energy filter at 20.0 eV slit
705 width. Tilt ranges were adjusted for each acquisition site to the minimum and maximum tilt
706 angles between -60° and +60° that encompassed the feature of interest. Tilt series were
707 acquired in 3° increments with each tilt image recorded over 5 movie frames at defocus
708 values between -4 to -8 µm. The total dose applied for each tilt series was ~100 e-/Å^2.

709 ***Tomogram Reconstruction and Analysis:***

710 Movie frames for each tilt series were motion corrected using MotionCor2 through
711 Relion 3.1 using 5x5 patches. Motion-corrected tilt series were generated using EMAN2. Tilt
712 series alignment, tomogram reconstruction, and CTF estimation were performed using the
713 automated EMAN2 pipeline. Feature segmentation was performed using neural network
714 training in EMAN2 or manually using IMOD 3dmod. Tomogram features were visualized and
715 analyzed using ChimeraX.

716 **Mevalonate bypass experiments**

717 **Azithromycin treatment:**

718 To generate PfAnchor^{Mev} iKD parasites with disrupted apicoplasts, Clone F3 parasites
719 were treated with 100 nM azithromycin (1× IC_{50}) (Sigma PZ0007) for one week, with
720 continuous supplementation of 50 µM mevalonate (Sigma M4667). The untreated parental
721 Anchor knockdown line served as a positive control for apicoplast genome detection (Table
722 S1).

723 **Measurement of parasite growth:**

724 To assess the dependence of apicoplast-intact and apicoplast-disrupted PfAnchor^{Mev}
725 iKD parasites on mevalonate for survival, asynchronous parasites were washed three times

726 with 10 mL of CMA to remove residual mevalonate and aTC. They were seeded in a 96-well
727 plate at an initial parasitemia of 0.5% and a hematocrit of 2%, with a total volume of 200 µL
728 per well. The parasites were then cultured under four conditions, with each condition tested
729 in quadruplicate: (1) CMA with 50 µM mevalonate and aTC, (2) CMA with 50 µM mevalonate,
730 (3) CMA with aTC, and (4) CMA alone. Cultures were incubated at 37°C in chambers gassed
731 with 94% N_2, 3% O_2, and 3% CO_2. Every other day, 10 µL of each sample was collected,
732 diluted 1:10 in phosphate-buffered saline (PBS), and stored in a 96-well plate at 4°C. To
733 prevent overgrowth, cultures were simultaneously diluted 1:8.

734 For growth curve determination, parasite samples were analyzed by flow cytometry
735 over two intervals: days 0 to 4 and days 5 to 8. On day 4, 10 µL of each diluted sample was
736 transferred to a new 96-well plate containing 100 µL of 1× SYBR Green (Invitrogen) in PBS per
737 well. The plates were incubated at room temperature in the dark with gentle shaking for 30
738 minutes. After staining, 150 µL of PBS was added to each well to dilute excess dye. The
739 samples were analyzed using an Attune Nxt flow cytometer (Thermo Fisher Scientific) with a
740 50-µL acquisition volume, a flow rate of 25 µL/min, and a total collection of 10,000 events
741 per sample. The same protocol was repeated on day 8 for the second set of samples
742 collected on days 6 and 8.

743 **Analysis of apicoplast genome**

744 To assess the integrity of the apicoplast genome after treatment with azithromycin,
745 PfAnchor^{Mev} iKD parasites were grown for 5 days in the presence of 100 nM azithromycin and
746 50 µM mevalonate before aTC washout. Genomic DNA was extracted using QIAmp DNA
747 blood mini kit (Qiagen, #51106) every two days up to day eight. Control samples from
748 PfAnchor^{Mev} iKD not treated with azithromycin were also collected. PCR analysis was
749 performed using primers oSAB484/oSAB485 (GAPDH, nuclear DNA), oSAB486/oSAB487
750 (tufa, apicoplast DNA), and oSAB488/oSAB489 (cytb3, mitochondrion DNA) as previously
751 described [77].

752 **Immunoprecipitation and proximal labeling**

753 ***Sample preparation***

754 Protein extraction for both immunoprecipitation (IP) and BioID experiments was
755 performed using the same lysis procedure. Parasites were cultured at 2% hematocrit and 4–
756 5% parasitemia before harvesting. Red blood cells were lysed using 0.05% saponin in PBS
757 supplemented with protease inhibitors (SigmaFast, Sigma S8820-20TAB) and incubated on
758 ice for 10 minutes. Parasites were washed three times with ice-cold PBS + protease
759 inhibitors by centrifugation at 10,000 g for 5 minutes at 4°C. The resulting pellets were
760 resuspended in 1 mL PBS + protease inhibitors, centrifuged at 10,000 rpm for 2 minutes at 4
761 °C, and stored at -80 °C or processed immediately. Parasite pellets were lysed in 1 mL RIPA
762 buffer (50 mM Tris-HCl pH 7.5, 150 mM NaCl, 1% NP-40, 0.5% sodium deoxycholate, 0.1%
763 SDS) supplemented with protease inhibitors. Samples were incubated on a rotator at 4 °C
764 for 30 minutes. To ensure efficient lysis, three rounds of sonication (30 seconds at 20
765 amplitude) were performed on ice, with 3-minute rest intervals between pulses. Lysates
766 were cleared by centrifugation at 15,000 g for 30 minutes at 4 °C, and the supernatant was
767 transferred to a fresh tube. For the MCMBP-BioID experiments, soluble and insoluble
768 fractions were processed separately using the same protocol described in our previous
769 study [39]. For immunoprecipitation, 50 µL of anti-V5 magnetic beads (Thermo, #88816) per
770 sample were washed twice with 1 mL RIPA buffer and incubated with the cleared lysates
771 overnight at 4 °C with constant rotation. Beads were collected using a magnetic stand,
772 washed three times with 50 mM ammonium bicarbonate buffer, and resuspended for on-
773 bead digestion and mass spectrometry analysis. For BioID, 50 µL of streptavidin magnetic
774 beads (Thermo, #88816) were used instead of V5 magnetic beads. After overnight
775 incubation, beads were washed following the same procedure as in IP before processing for
776 mass spectrometry analysis.

777 ***On bead digests:***

778 After washing, beads were covered with 8 M Urea, 100 mM Tris hydrochloride, pH 8.5,
779 reduced with 5 mM tris (2-carboxyethyl) phosphine hydrochloride (TCEP, Sigma-Aldrich Cat
780 No: C4706) for 30 minutes at room temperature to reduce the disulfide bonds. The resulting
781 free cysteine thiols were alkylated using 10 mM choloracetamide (CAA, Sigma Aldrich Cat
782 No: C0267) for 30 minutes at RT, protected from light. Samples were diluted to 2 M Urea with

783 50 mM Tris pH 8.5 and proteolytic digestion was carried out with Trypsin/LysC Gold (0.4 µg,
784 Mass Spectrometry grade, Promega Corporation Cat No: V5072) overnight at 35 °C. After
785 digestion, samples were quenched with 0.4% trifluoroacetic acid (v/v, Fluka Cat No: 91699).
786 Samples were either injected onto a trap column followed by analytical column or first
787 subjected to a solid phase extraction clean up on Pierce C18 spin columns (Cat No 87870).

788 ***Liquid Chromatography Mass Spectrometry:***

789 Approximately 1/15th of each IP sample was loaded onto a 5 cm C18 trap column
790 Acclaim™ PepMap™ 100 (3 µm particle size, 75 µm diameter; Thermo Scientific, Cat No:
791 164946) followed by a 25 cm EASY-Spray column (Thermo Scientific, Cat No: ES902) and
792 analyzed using a Q-Exactive Plus mass spectrometer (Thermo Fisher Scientific) operated in
793 positive ion mode. Solvent B was increased from 5%-35% over 100 min, to 90% over 2 min,
794 back to 3% over 2 minutes (Solvent A: 95% water, 5% acetonitrile, 0.1% formic acid; Solvent
795 B: 100% acetonitrile, 0.1% formic acid). A data dependent top 15 method was used with MS
796 scan range of 350-2000 m/z, resolution of 70,000, automatic gain control (AGC) target 3e6,
797 maximum injection time (IT) of 200 ms. MS2 resolution of 17,500, scan range of 200-2000
798 m/z, normalized collision energy of 30, isolation window of 4 m/z, target AGC of 1e5, and
799 maximum IT of 150 ms. Dynamic exclusion of 10 sec, charge exclusion of 1, 7, 8, >8 and
800 isotopic exclusion parameters were used. For samples post C18 cleanup, after drying in a
801 speed vacuum, samples were resuspended in 25 µL 0.1 % FA. Approximately 1/5th of each
802 sample was then injected using an EasyNano1200 LC coupled to an Exploris 480 orbitrap
803 mass spectrometer (Thermo Fisher Scientific)). Solvent B (80% Acetonitrile, 0.1 % FA) was
804 increased from 8-35 % over 90 minutes, increased from 35-65 % over 15 min, increased to
805 85% over 5 min, held at 85% for 5 min, and decreased to 4% over 5 min. The mass
806 spectrometer was operated in positive ion mode, advanced peak determination on, default
807 charge state of 2 and user defined lock mass of 445.12003. 4 second cycle time was used
808 with MS1 parameters of scan range 375-1500 m/z: orbitrap resolution of 60,000, standard
809 AGC, automatic max IT, and RF lens of 40%. Monoisotopic peak determination was set to
810 peptide with a minimum intensity filter of 5e3, charge state filter of 2-7, and dynamic
811 exclusion of 30 s with 5 ppm mass tolerance. MS2 parameters included an isolation window

812 of 4 m/z, normalized high energy dissociation energy of 30 %, orbitrap resolution of 15,000,
813 user defined first mass of 110 m/z, standard AGC target and auto max IT. Data were recorded
814 using Tune application 4.2.362.42.

815 ***Data analysis:***

816 Data were analyzed using Proteome Discoverer 2.5.0.400 (Thermo Fisher Scientific).
817 *Plasmodium falciparum* 3D7 and *Homo sapiens* reference proteome databases
818 (downloaded from Uniprot on 04/06/2021 with 5381 sequences and on 05/13/2022 with
819 78806 sequences respectively), plus common laboratory contaminants (73 sequences)
820 were searched using SEQUEST HT. Precursor mass tolerance was set to 10 ppm and
821 fragment mass tolerance set at 0.02 Da with a maximum of 3 missed cleavages. A maximum
822 of 3 modifications were allowed per peptide. Dynamic modifications included methionine
823 oxidation; phosphorylation on serine, threonine, and tyrosine; dynamic protein terminus
824 modifications were acetylation, met-loss, and met-loss plus acetylation. Static
825 modifications were carbamidomethylation on cysteines. Percolator false discovery rate
826 (FDR) filtration of 1% was applied to both the peptide-spectrum match and protein levels.
827 Search results were loaded into Scaffold Q + S Software (version 5.2.2, Proteome Software,
828 Inc) for visualization.

829

830 **Data availability**

831 Raw and processed mass spectrometry data have been uploaded to ProteomeXchange
832 with accession PXD062126.

833 **Author contributions**

834 **James Blauwkamp:** Methodology, Formal analysis, Investigation, Data curation, Writing -
835 Original Draft, Writing - Review & Editing, Visualization.

836 **Krithika Rajaram:** Methodology, Investigation, Data curation, Visualization, Review &
837 Editing

838 **Sophia R. Staggers:** Methodology, Investigation, Data curation, Visualization, Review &
839 Editing.

Oliver Harrigan: Methodology**,** Data curation.

Emma H. Doud: Methodology, Formal analysis Data curation, Review & Editing

Sean T. Prigge: Review & Editing, Funding Acquisition.

Stella Y. Sun: Methodology, Formal analysis, Investigation, Data curation, Resources, Review & Editing, Supervision**.**

Sabrina Absalon: Conceptualization, Methodology, Formal analysis, Investigation, Data curation, Visualization, Resources, Writing – Review & Editing, Supervision, Project administration, Funding Acquisition.

Acknowledgements

We thank Michael Holmes and Anat Florentin for insightful discussions and review of the manuscript. We thank BEI Resources (NIAID, NIH), the European Malaria Reagent Repository, and Vasant Muralidharan for the provision of antibodies. This research made use of PlasmoDB, a VEuPathDB resource [78]. This research was supported by Grant No. 2023198 from the United States-Israel Binational Science Foundation (BSF) and was made possible by an award from the Indiana University School of Medicine (S.A., BRG award no. EPAR2216). The content is solely the responsibility of the authors and does not necessarily represent the official views of the Indiana University School of Medicine. This research was also supported by S.T.P. from the National Institutes of Health (R01 AI125534), the Johns Hopkins Malaria Research Institute, and Bloomberg Philanthropies, with S.T.P. as principal investigator. The mass spectrometry work performed in this work was done by the Indiana University School of Medicine Proteomics Core and supported by Start-up funds from S.A. Acquisition of the IUSM Proteomics core instrumentation used for this project was provided by the Indiana University Precision Health Initiative**.** The proteomics work was supported, in part, by the Indiana Clinical and Translational Sciences Institute (funded in part by Award Number UL1TR002529 from the National Institutes of Health, National Center for Advancing Translational Sciences, Clinical and Translational Sciences Award) and, in part, by the IU Simon Comprehensive Cancer Center Support Grant (Award Number P30CA082709 from the National Cancer Institute). The Pittsburgh Center for CryoEM (RRID:SCR_025216) used for data collection in this project was supported, in part, by the University of Pittsburgh, the

School of Medicine, the Department of Structural Biology, and the National Institutes of Health (grants S10-OD-019995 and S10-OD-025009).

References:

1. Burki, F., et al., *The New Tree of Eukaryotes*. Trends in Ecology & Evolution, 2020. **35**(1): p. 43-55.
2. Collier, S.L., et al., *Modes and mechanisms for the inheritance of mitochondria and plastids in pathogenic protists*. PLOS Pathogens, 2025. **21**(1): p. e1012835.
3. Lewis, W.H., et al., *Plastid translocon recycling in dinoflagellates demonstrates the portability of complex plastids between hosts*. Current Biology, 2024. **34**(23): p. 5494-5506.e3.
4. Gray, M.W., *The endosymbiont hypothesis revisited*. Int Rev Cytol, 1992. **141**: p. 340, 221-242.
5. Gould, S.B., R.F. Waller, and G.I. McFadden, *Plastid evolution*. Annu Rev Plant Biol, 2008. **59**: p. 491-517.
6. Goodman, C.D., H.D. Buchanan, and G.I. McFadden, *Is the Mitochondrion a Good Malaria Drug Target?* Trends in Parasitology, 2017. **33**(3): p. 185-193.
7. Low, L.M., D.I. Stanisic, and M.F. Good, *Exploiting the apicoplast: apicoplast-targeting drugs and malaria vaccine development*. Microbes and Infection, 2018. **20**(9): p. 477-483.
8. Organization, W.H., *World Malaria Report 2023*. 2023. 1-356.
9. Gerald, N., B. Mahajan, and S. Kumar, *Mitosis in the human malaria parasite Plasmodium falciparum*. Eukaryotic cell, 2011. **10**(4): p. 474-482.
10. Köhler, S., et al., *A Plastid of Probable Green Algal Origin in Apicomplexan Parasites*. Science, 1997. **275**(5305): p. 1485-1489.
11. Janouškovec, J., et al., *A common red algal origin of the apicomplexan, dinoflagellate, and heterokont plastids*. Proceedings of the National Academy of Sciences, 2010. **107**(24): p. 10949-10954.
12. Fast, N.M., et al., *Nuclear-Encoded, Plastid-Targeted Genes Suggest a Single Common Origin for Apicomplexan and Dinoflagellate Plastids*. Molecular Biology and Evolution, 2001. **18**(3): p. 418-426.
13. Yeh, E. and J.L. DeRisi, *Chemical Rescue of Malaria Parasites Lacking an Apicoplast Defines Organelle Function in Blood-Stage Plasmodium falciparum*. PLOS Biology, 2011. **9**(8): p. e1001138.
14. Okada, M., et al., *Critical role for isoprenoids in apicoplast biogenesis by malaria parasites*. eLife, 2022. **11**: p. e73208.

15. Kennedy, K., et al., *Delayed death in the malaria parasite Plasmodium falciparum is caused by disruption of prenylation-dependent intracellular trafficking.* PLOS Biology, 2019. **17**(7): p. e3000376.
16. Swift, R.P., et al., *Dephospho-CoA kinase, a nuclear-encoded apicoplast protein, remains active and essential after Plasmodium falciparum apicoplast disruption.* Embo j, 2021. **40**(16): p. e107247.
17. Ralph, S.A., et al., *Metabolic maps and functions of the Plasmodium falciparum apicoplast.* Nature Reviews Microbiology, 2004. **2**(3): p. 203-216.
18. Buchanan, H.D., C.D. Goodman, and G.I. McFadden, *Roles of the apicoplast across the life cycles of rodent and human malaria parasites.* J Eukaryot Microbiol, 2022. **69**(6): p. e12947.
19. Gisselberg, J.E., et al., *The suf iron-sulfur cluster synthesis pathway is required for apicoplast maintenance in malaria parasites.* PLoS Pathog, 2013. **9**(9): p. e1003655.
20. Waller, R.F., et al., *Protein trafficking to the plastid of Plasmodium falciparum is via the secretory pathway.* Embo j, 2000. **19**(8): p. 1794-802.
21. Liffner, B., et al., *Atlas of Plasmodium falciparum intraerythrocytic development using expansion microscopy*. 2023, eLife Sciences Publications, Ltd.
22. Rudlaff, R.M., et al., *Three-dimensional ultrastructure of Plasmodium falciparum throughout cytokinesis.* PLOS Pathogens, 2020. **16**(6): p. e1008587.
23. Morano Alexander, A., et al., *The dynamin-related protein PfDyn2 is essential for both apicoplast and mitochondrial fission in Plasmodium falciparum.* mBio, 2024. **16**(1): p. e03036-24.
24. Thakur, V., et al., *A dynamin-like protein in Plasmodium falciparum plays an essential role in parasite growth, mitochondrial development and homeostasis during asexual blood stages.* Biochimica et Biophysica Acta (BBA) - Molecular Cell Research, 2025: p. 119940.
25. Bui, H.T. and J.M. Shaw, *Dynamin assembly strategies and adaptor proteins in mitochondrial fission.* Curr Biol, 2013. **23**(19): p. R891-9.
26. Koirala, S., et al., *Interchangeable adaptors regulate mitochondrial dynamin assembly for membrane scission.* Proceedings of the National Academy of Sciences, 2013. **110**(15): p. E1342-E1351.
27. Zerihun, M., S. Sukumaran, and N. Qvit, *The Drp1-Mediated Mitochondrial Fission Protein Interactome as an Emerging Core Player in Mitochondrial Dynamics and Cardiovascular Disease Therapy.* Int J Mol Sci, 2023. **24**(6).
28. Gandre-Babbe, S. and A.M. van der Bliek, *The novel tail-anchored membrane protein Mff controls mitochondrial and peroxisomal fission in mammalian cells.* Mol Biol Cell, 2008. **19**(6): p. 2402-12.
29. Palmer, C.S., et al., *MiD49 and MiD51, new components of the mitochondrial fission machinery.* EMBO Rep, 2011. **12**(6): p. 565-73.
30. Stojanovski, D., et al., *Levels of human Fis1 at the mitochondrial outer membrane regulate mitochondrial morphology.* Journal of Cell Science, 2004. **117**(7): p. 1201-1210.
31. Zhao, J., et al., *Human MIEF1 recruits Drp1 to mitochondrial outer membranes and promotes mitochondrial fusion rather than fission.* Embo j, 2011. **30**(14): p. 2762-78.

952 32. Griffin, E.E., J. Graumann, and D.C. Chan, *The WD40 protein Caf4p is a component*
953 *of the mitochondrial fission machinery and recruits Dnm1p to mitochondria*. J Cell
954 Biol, 2005. **170**(2): p. 237-48.
955 33. Mozdy, A.D., J.M. McCaffery, and J.M. Shaw, *Dnm1p GTPase-mediated*
956 *mitochondrial fission is a multi-step process requiring the novel integral membrane*
957 *component Fis1p*. J Cell Biol, 2000. **151**(2): p. 367-80.
958 34. Tieu, Q. and J. Nunnari, *Mdv1p is a WD repeat protein that interacts with the*
959 *dynamin-related GTPase, Dnm1p, to trigger mitochondrial division*. J Cell Biol, 2000.
960 **151**(2): p. 353-66.
961 35. Jacobs, K., R. Charvat, and G. Arrizabalaga, *Identification of Fis1 Interactors in*
962 *Toxoplasma gondii Reveals a Novel Protein Required for Peripheral Distribution of*
963 *the Mitochondrion*. mBio, 2020. **11**(1).
964 36. Oliveira Souza, R.O., et al., *IMC10 and LMF1 mediate mitochondrial morphology*
965 *through mitochondrion-pellicle contact sites in Toxoplasma gondii*. J Cell Sci, 2022.
966 **135**(22).
967 37. Maruthi, M., et al., *Dispensable Role of Mitochondrial Fission Protein 1 (Fis1) in the*
968 *Erythrocytic Development of Plasmodium falciparum*. mSphere, 2020. **5**(5).
969 38. Ganesan, S.M., et al., *Synthetic RNA–protein modules integrated with native*
970 *translation mechanisms to control gene expression in malaria parasites*. 2016. **7**(1):
971 p. 10727.
972 39. Absalon, S. and J.D. Dvorin, *Depletion of the mini-chromosome maintenance*
973 *complex binding protein allows the progression of cytokinesis despite abnormal*
974 *karyokinesis during the asexual development of Plasmodium falciparum*. Cell
975 Microbiol, 2021. **23**(3): p. e13284.
976 40. Jumper, J., et al., *Highly accurate protein structure prediction with AlphaFold*.
977 Nature, 2021. **596**(7873): p. 583-589.
978 41. Holm, L., *Dali server: structural unification of protein families*. Nucleic Acids
979 Research, 2022. **50**(W1): p. W210-W215.
980 42. Behrens, H.M. and T. Spielmann, *Identification of domains in Plasmodium*
981 *falciparum proteins of unknown function using DALI search on AlphaFold*
982 *predictions*. Sci Rep, 2024. **14**(1): p. 10527.
983 43. Viswanathan, S., et al., *High-performance probes for light and electron microscopy*.
984 Nat Methods, 2015. **12**(6): p. 568-76.
985 44. Chappell, L., et al., *Refining the transcriptome of the human malaria parasite*
986 *Plasmodium falciparum using amplification-free RNA-seq*. BMC Genomics, 2020.
987 **21**(1): p. 395.
988 45. Swift, R.P., et al., *A mevalonate bypass system facilitates elucidation of plastid*
989 *biology in malaria parasites*. PLOS Pathogens, 2020. **16**(2): p. e1008316.
990 46. Taylor, H.M., et al., *The malaria parasite cyclic GMP-dependent protein kinase plays*
991 *a central role in blood-stage schizogony*. Eukaryot Cell, 2010. **9**(1): p. 37-45.
992 47. Das, S., et al., *Multiple essential functions of Plasmodium falciparum actin-1 during*
993 *malaria blood-stage development*. BMC Biology, 2017. **15**(1): p. 70.

48. Michal, S., et al., *Organelle Development and Inheritance are Driven by Independent Nuclear and Organellar Mechanisms in Malaria Parasites*. bioRxiv, 2025: p. 2025.03.06.641809.
49. Verhoef, J.M.J., et al., *Detailing organelle division and segregation in Plasmodium falciparum*. Journal of Cell Biology, 2024. **223**(12): p. e202406064.
50. Gurnett, A.M., et al., *Purification and molecular characterization of cGMP-dependent protein kinase from Apicomplexan parasites. A novel chemotherapeutic target*. J Biol Chem, 2002. **277**(18): p. 15913-22.
51. Dahl, E.L., et al., *Tetracyclines specifically target the apicoplast of the malaria parasite Plasmodium falciparum*. Antimicrob Agents Chemother, 2006. **50**(9): p. 3124-31.
52. Sidhu, A.B.S., et al., *In Vitro Efficacy, Resistance Selection, and Structural Modeling Studies Implicate the Malarial Parasite Apicoplast as the Target of Azithromycin**. Journal of Biological Chemistry, 2007. **282**(4): p. 2494-2504.
53. Elwi, A.N., et al., *Mitochondrial chaperone DnaJA3 induces Drp1-dependent mitochondrial fragmentation*. Int J Biochem Cell Biol, 2012. **44**(8): p. 1366-76.
54. Barth, J., T. Schach, and J.M. Przyborski, *HSP70 and their co-chaperones in the human malaria parasite P. falciparum and their potential as drug targets*. Frontiers in Molecular Biosciences, 2022. **9**.
55. Stortz, J.F., et al., *Formin-2 drives polymerisation of actin filaments enabling segregation of apicoplasts and cytokinesis in Plasmodium falciparum*. eLife, 2019. **8**: p. e49030.
56. Rudlaff, R.M., et al., *An essential contractile ring protein controls cell division in Plasmodium falciparum*. Nat Commun, 2019. **10**(1): p. 2181.
57. Singh, N., et al., *Redefining the specificity of phosphoinositide-binding by human PH domain-containing proteins*. Nature Communications, 2021. **12**(1): p. 4339.
58. Tawk, L., et al., *Phosphatidylinositol 3-phosphate, an essential lipid in Plasmodium, localizes to the food vacuole membrane and the apicoplast*. Eukaryot Cell, 2010. **9**(10): p. 1519-30.
59. Dans, M.G., et al., *Sulfonylpiperazine compounds prevent Plasmodium falciparum invasion of red blood cells through interference with actin-1/profilin dynamics*. PLoS Biol, 2023. **21**(4): p. e3002066.
60. Gareus, R., et al., *Mouse Profilin 2 Regulates Endocytosis and Competes with SH3 Ligand Binding to Dynamin 1 **. Journal of Biological Chemistry, 2006. **281**(5): p. 2803-2811.
61. Velle, K.B., et al., *Actin network evolution as a key driver of eukaryotic diversification*. Journal of Cell Science, 2024. **137**(15): p. jcs261660.
62. Witke, W., et al., *In mouse brain profilin I and profilin II associate with regulators of the endocytic pathway and actin assembly*. Embo j, 1998. **17**(4): p. 967-76.
63. Hopkins, J., et al., *The plastid in Plasmodium falciparum asexual blood stages: a three-dimensional ultrastructural analysis*. Protist, 1999. **150**(3): p. 283-95.
64. Lim, L. and G.I. McFadden, *The evolution, metabolism and functions of the apicoplast*. Philos Trans R Soc Lond B Biol Sci, 2010. **365**(1541): p. 749-63.

65. Sun, S.Y., et al., *Cryogenic electron tomography reveals novel structures in the apical complex of Plasmodium falciparum*. mBio, 2024. **15**(4): p. e0286423.
66. Floris, D. and W. Kühlbrandt, *Molecular landscape of etioplast inner membranes in higher plants*. Nat Plants, 2021. **7**(4): p. 514-523.
67. Xu, W., et al., *Inheritance of the genome-less apicoplast in the "apicoplast-minus" Plasmodium falciparum*. bioRxiv, 2025.
68. Shonhai, A., A. Boshoff, and G.L. Blatch, *The structural and functional diversity of Hsp70 proteins from Plasmodium falciparum*. Protein Science, 2007. **16**(9): p. 1803-1818.
69. Blauwkamp, J., et al., *Nuclear pore complexes undergo Nup221 exchange during blood-stage asexual replication of Plasmodium parasites*. mSphere, 2024. **9**(12): p. e00750-24.
70. Lasonder, E., et al., *Integrated transcriptomic and proteomic analyses of P. falciparum gametocytes: molecular insight into sex-specific processes and translational repression*. Nucleic Acids Res, 2016. **44**(13): p. 6087-101.
71. López-Barragán, M.J., et al., *Directional gene expression and antisense transcripts in sexual and asexual stages of Plasmodium falciparum*. BMC Genomics, 2011. **12**: p. 587.
72. Frischknecht, F. and K. Matuschewski, *Plasmodium Sporozoite Biology*. Cold Spring Harb Perspect Med, 2017. **7**(5).
73. Trager, W. and J.B. Jensen, *Human Malaria Parasites in Continuous Culture*. Science, 1976. **193**(4254): p. 673-675.
74. Gurung, P., P. McGee James, and D. Dvorin Jeffrey, *PfCAP-H is essential for assembly of condensin I complex and karyokinesis during asexual proliferation of Plasmodium falciparum*. mBio, 2024. **15**(5): p. e02850-23.
75. Absalon, S., J.A. Robbins, and J.D. Dvorin, *An essential malaria protein defines the architecture of blood-stage and transmission-stage parasites*. 2016. **7**(1): p. 11449.
76. Liffner, B., et al., *PfCERLI1 is a conserved rhoptry associated protein essential for Plasmodium falciparum merozoite invasion of erythrocytes*. Nature Communications, 2020. **11**(1): p. 1411.
77. Pasaje, C.F.A., et al., *Selective inhibition of apicoplast tryptophanyl-tRNA synthetase causes delayed death in Plasmodium falciparum*. Scientific Reports, 2016. **6**(1): p. 27531.
78. Amos, B., et al., *VEuPathDB: the eukaryotic pathogen, vector and host bioinformatics resource center*. Nucleic Acids Research, 2022. **50**(D1): p. D898-D911.

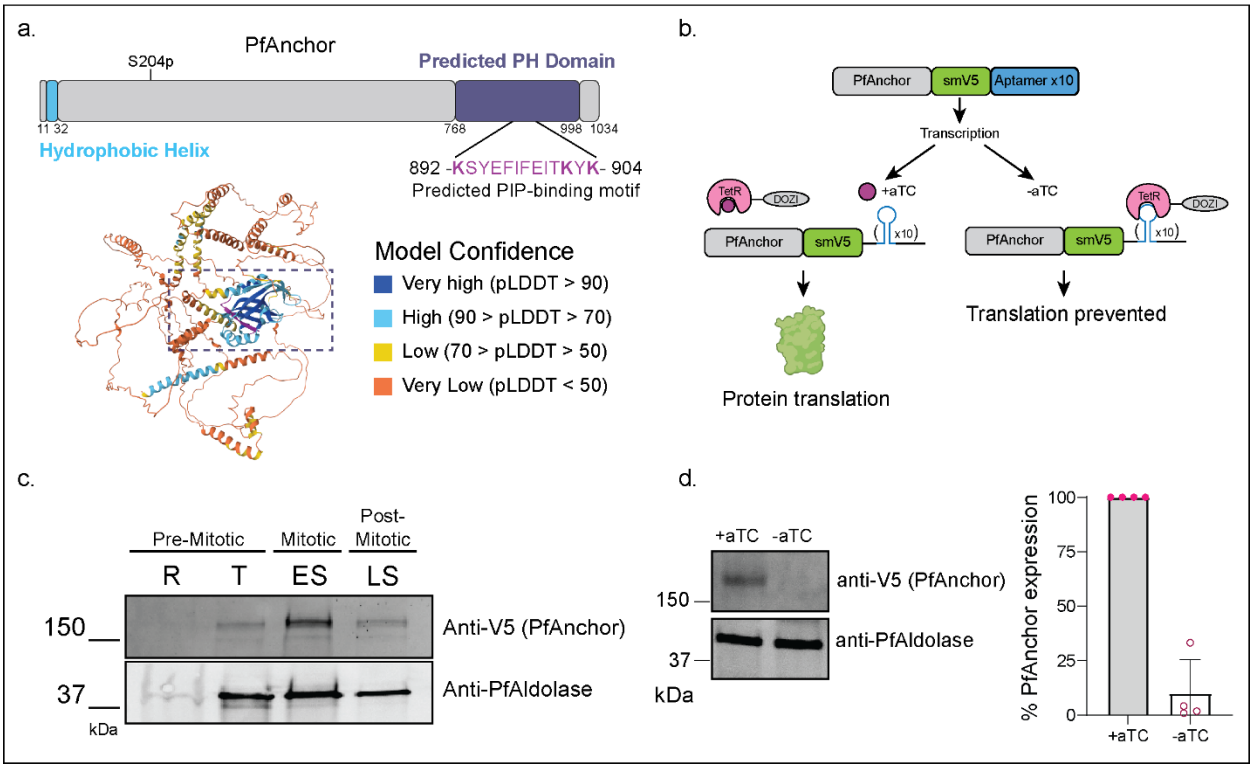

Figure 1: PfAnchor is an essential conserved *Plasmodium* protein expressed through the asexual life cycle.

a. Schematic representation of PfAnchor's structural features and predicted protein folding. PfAnchor primary sequence shows a single phosphorylation site at S204. Alphafold3 modeling combined with a DALI protein domain search identified a conserved pleckstrin homology (PH) domain (PfAnchor AA 768-998) across *Plasmodium* species. The sequence alignment of this region shows strong conservation, with a predicted phosphoinositides (PIP)-binding motif (PfAnchor AA 892-904) highlighted in magenta in the structural model. **b.** Schematic of PfAnchor tagging strategy and conditional knockdown system. PfAnchor was tagged with an smV5 epitope for visualization, and knockdown was achieved using the TetR-aptamer system, where protein translation depends on anhydrotetracycline (aTC) availability. **c.** Representative western blot (N=2) of parasite protein lysates from ring (R), trophozoite (T), early schizont (ES), and late schizont (LS) stages. Anti-V5 detects PfAnchor, showing that it is expressed throughout the asexual life cycle with highest abundance in schizont stages. Anti-PfAldolase is used as a loading control, as it is a constitutively expressed cytoplasmic protein that maintains relatively stable levels across all intraerythrocytic stages. **d.** Western blot analysis confirming PfAnchor knockdown efficiency. Quantification performed via measurement of the fluorescent intensities of the sample (V5) bands compared to the normalized intensities of the loading control (PfAldolase) bands. Plotted is mean +/- SD, n = four biological replicates.

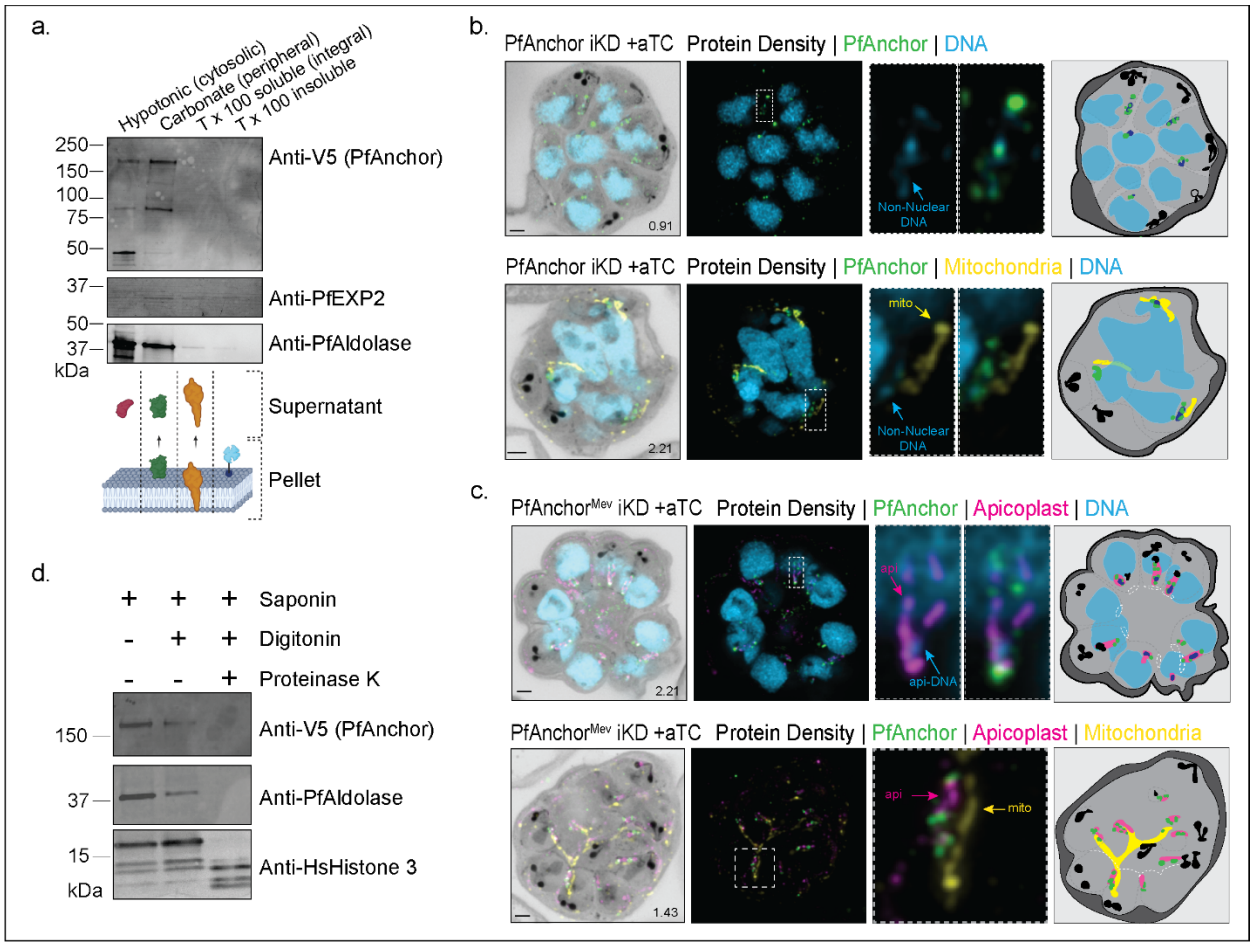

Figure 2: PfAnchor localizes to the cytoplasmic side of the apicoplast outer membrane.
a. Sodium carbonate fractionation assay demonstrating that PfAnchor is peripherally associated with a membrane. Fractions include hypotonic (unbound cytoplasmic proteins), carbonate (peripherally bound membrane proteins), Triton X-100 soluble (integral membrane proteins), and Triton X-100 insoluble (GPI-anchored membrane proteins). PfAldolase was used as a cytoplasmic control, PfEXP2 was used as peripheral membrane control. **b-c.** U-EXM analysis of PfAnchor localization in PfAnchor-iKD and PfAnchor^{Mev}-iKD cell lines. PfAnchor is detected in close proximity to non-nuclear DNA but does not colocalize with mitochondrial DNA. Apicoplast staining confirms that PfAnchor is specifically localized around the apicoplast. Protein density is shown in grayscale, PfAnchor in green, apicoplast in magenta, mitochondria in yellow, and DNA in blue. Scale bars: 2 µm, with image depth (µm) indicated. Schematic representations highlight non-nuclear DNA (dark blue) and basal complexes (white), with light gray dashed lines marking areas of potential membrane staining based on NHS ester density changes. **d.** Proteinase K protection assay shows that the C-terminal tagged PfAnchor is cytoplasmically exposed. Anti-PfAldolase and anti-HsHistone H3 were used as unprotected and protected controls, respectively.

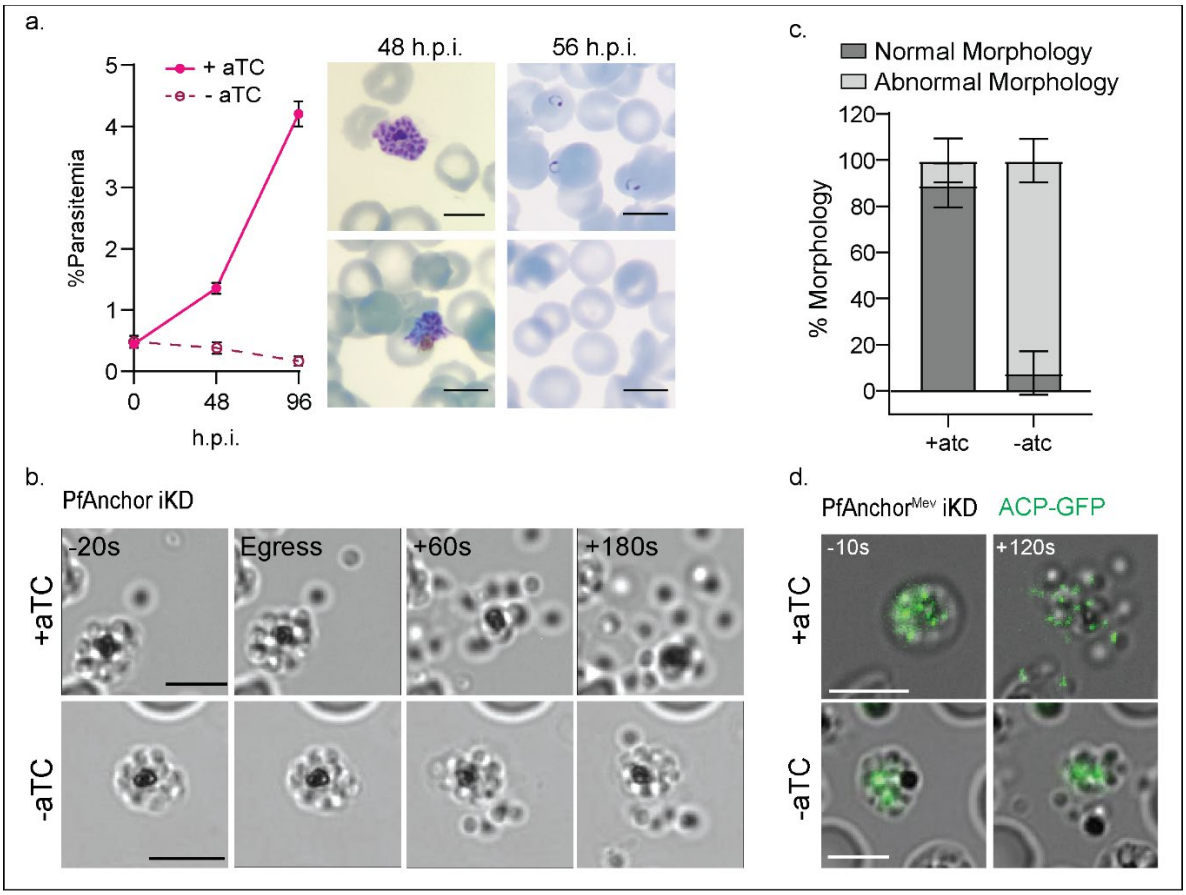

Figure 3: PfAnchor is required for proper parasite cytokinesis but dispensable for egress.
a. Growth analysis of PfAnchor expressing and deficient parasites over two replication cycles. Parasitemia was quantified by light microscopy over three biological replicates. Hemacolor-stained smears show late-stage parasites with abnormal morphology prior to egress and absence of ring stage parasites following egress. Scale bar 5 µm. **b.** Representative live microscopy images of PfAnchor-expressing (top) and PfAnchor-deficient (bottom) parasites at the point of egress. While PfAnchor-expressing parasites display daughter merozoites dispersing away from each other, PfAnchor-deficient parasites exhibit daughter merozoites remaining clumped together (abnormal morphology). Scale bar 5 µm. **c.** Quantification of normal and abnormal morphology of daughter parasites following egress from the live microscopy experiments over three biological replicates. PfAnchor-expressing parasites showed 89.3 +/- 9.5% normal morphology over 3 replicates while the PfAnchor-deficient parasites showed 10.7 +/- 9.3% normal morphology over 3 replicates. **d.** Representative live microscopy images of PfAnchor-expressing (top) and PfAnchor-deficient (bottom) parasites at the point of egress with the apicoplast shown in green. Parasites expressing PfAnchor show daughters that are moving away from each other with the apicoplast labeled in green (ACP-GFP). In PfAnchor-expressing parasites, daughter cells separate with apicoplast fragments properly inherited by individual merozoites. In contrast, PfAnchor-deficient parasites display daughter cells remaining clumped together, with a single apicoplast strand persisting across the cluster. Scale bar 5 µm.

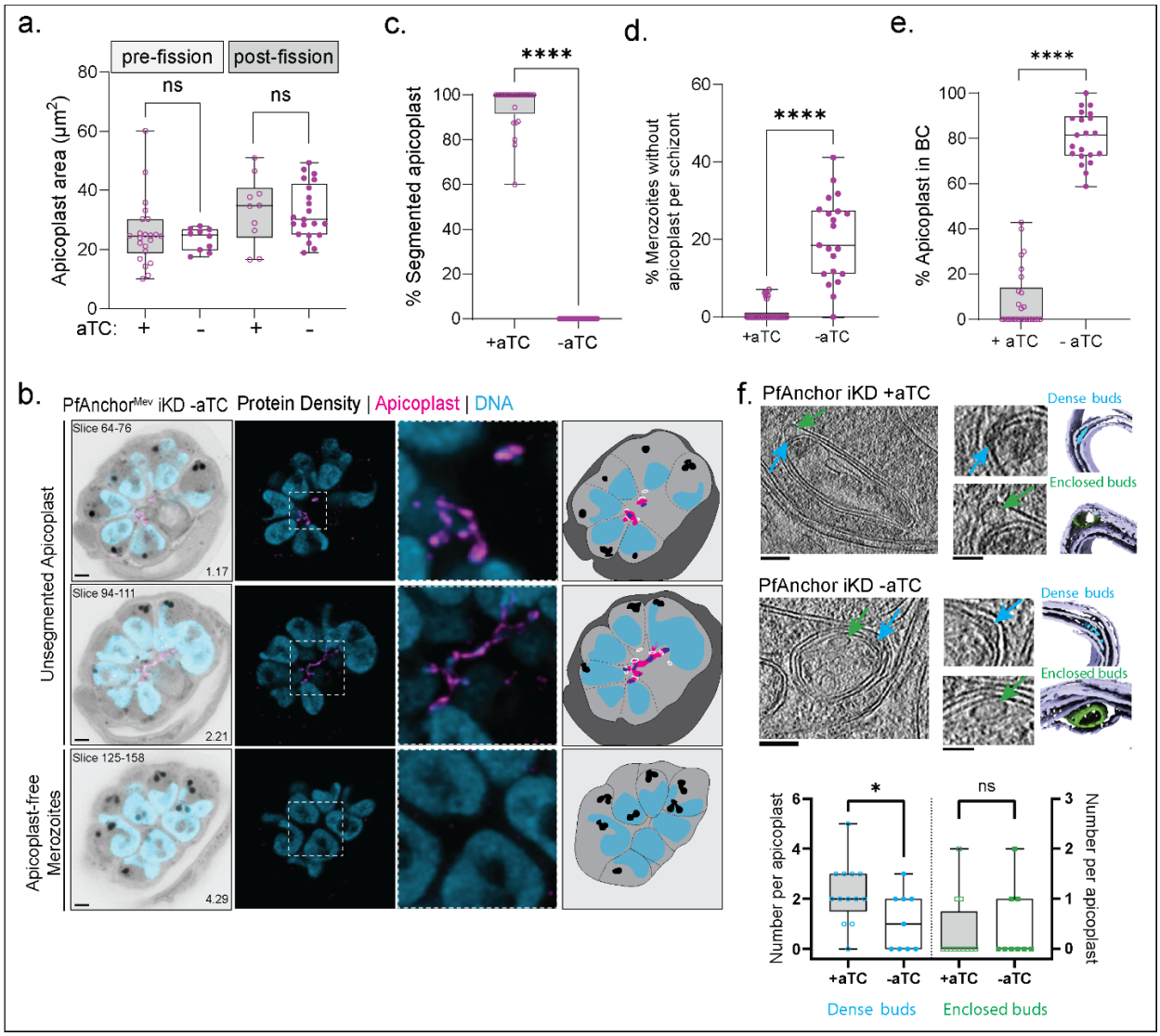

Figure 4: PfAnchor is required for apicoplast division and inheritance but not biogenesis.
a. Quantification of total apicoplast area in age-matched pre- and post-division parasites shows no significant differences between PfAnchor-expressing and PfAnchor-deficient parasites, indicating that apicoplast biogenesis is unaffected (unpaired t-tests, +aTC: 32 cells over 2 replicates, -aTC 31 cells over 2 replicates, not significant). **b.** Representative images illustrating the quantified phenotype in (c-e). Shown are different z-slices of a single PfAnchor-deficient parasite displaying apicoplast signal trapped within the basal complex, an unsegmented apicoplast, and daughter parasites devoid of apicoplast signal. Protein density in grayscale, apicoplast in pink and DNA in blue. Scale bar 2 µm. Z-slices used are indicated, with image depth (µm) noted. **c.** Percentage of daughter parasites per schizont with a fully segmented apicoplast in schizonts stalled at the end of segmentation. Unpaired t-tests, +aTC: 25 cells over 3 replicates, -aTC: 21 cells over 3 replicates, **** indicates p-value < 0.0001. **d.** Percentage of daughter parasites lacking apicoplast signal in schizonts stalled at the end of schizogony. Unpaired t-tests, +aTC: 25 cells over 3 replicates, -aTC: 21 cells over 3 replicates, **** indicates p-value < 0.0001. **e.** Percentage of daughter parasites per schizont

exhibiting apicoplast signal within the basal complex (BC) in schizonts stalled at the end of schizogony. Unpaired t-tests, +aTC: 25 cells over 3 replicates, -aTC: 21 cells over 3 replicates, **** indicates p-value < 0.0001. **f.** Representative cryo-electron tomography (cryo-ET) images showing that PfAnchor depletion does not affect apicoplast membrane integrity. However, analysis of internal apicoplast structures reveals a significant reduction in the number of dense intermembrane buds (blue arrows and data points) upon PfAnchor knockdown, while enclosed membrane buds (green arrows and data points) remain unaffected. Scale bars: 100 nm (unpaired t-tests, * indicates p-value < 0.05).

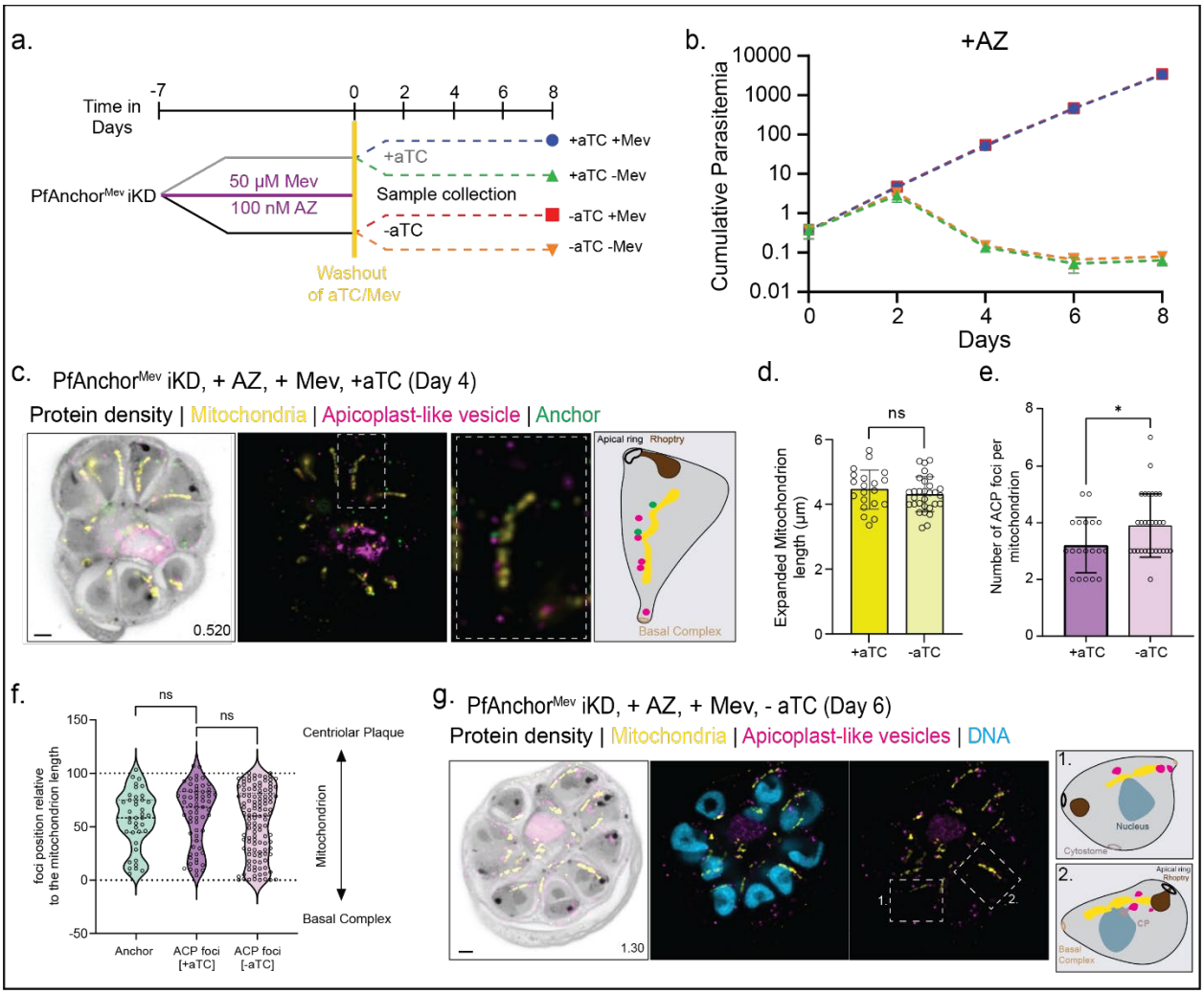

Figure 5: Disruption of apicoplast branching rescues PfAnchor-deficient parasites, while apicoplast-like vesicle distribution along mitochondria remain unchanged.

a. Schematic of the experimental setup. PfAnchor^{Mev} iKD parasites were pre-treated with mevalonate (+Mev) and azithromycin (+AZ) for 7 days to disrupt the apicoplast structure, leading to the formation of apicoplast-like vesicles. Following this pre-treatment, parasites were washed and maintained under the indicated conditions (±aTC, ±Mev) for downstream analyses. **b.** Cumulative parasitemia of PfAnchor-expressing (+aTC) and PfAnchor-deficient (-aTC) parasites over 8 days in +AZ conditions. In AZ-treated parasites, disruption of the apicoplast resulted in the formation of apicoplast-like vesicles, which rescued the growth defect of PfAnchor-deficient parasites, but only in the presence of mevalonate (+Mev). Parasites lacking both PfAnchor and mevalonate (-Mev) failed to propagate. Parasites were sampled every 2 days for growth and PCR analysis, with cultures diluted at 1:8 every 2 days to ensure continued replication. Data represent mean ± SD from 2 biological replicates in quadruplicate. **C**. Representative U-ExM image of a PfAnchor-expressing parasite displaying apicoplast-like vesicles (pink, anti-GFP) within the forming daughter parasites, along with PfAnchor (green, anti-V5) and mitochondria (yellow, anti-Hsp60). Protein density is shown in grayscale. Scale bar: 2 µm, with z-slices and image depth (µm) indicated. **d.** Quantification of mitochondrial length in

PfAnchor-expressing (8 cells, 15 mitochondria) and PfAnchor-deficient (10 cells, 30 mitochondria) parasites following AZ treatment. No significant differences in mitochondrial length were observed between conditions (ns, unpaired t-test). (**e-g**)**.** Apicoplast-like vesicles were analyzed for their association with mitochondria. **e**. The number of apicoplast-like vesicles associated with mitochondria was significantly increased in PfAnchor-deficient (-aTC) parasites compared to PfAnchor-expressing (+aTC) parasites. **f**. Violin plots show the spatial distribution of apicoplast-like vesicles along the mitochondria, demonstrating that PfAnchor depletion does not alter their positioning. Statistical analysis was performed using unpaired t-tests, +aTC: 20 mitochondria from 8 schizonts; -aTC: 30 mitochondria from 15 schizonts. **g**. Representative U-ExM image of a PfAnchor-deficient parasite showing apicoplast-like vesicles (pink, anti-GFP) within forming daughter parasites, along with mitochondria (yellow, anti-Hsp60). Protein density is shown in grayscale. Scale bar: 2 µm, with z-slices and image depth (µm) indicated.

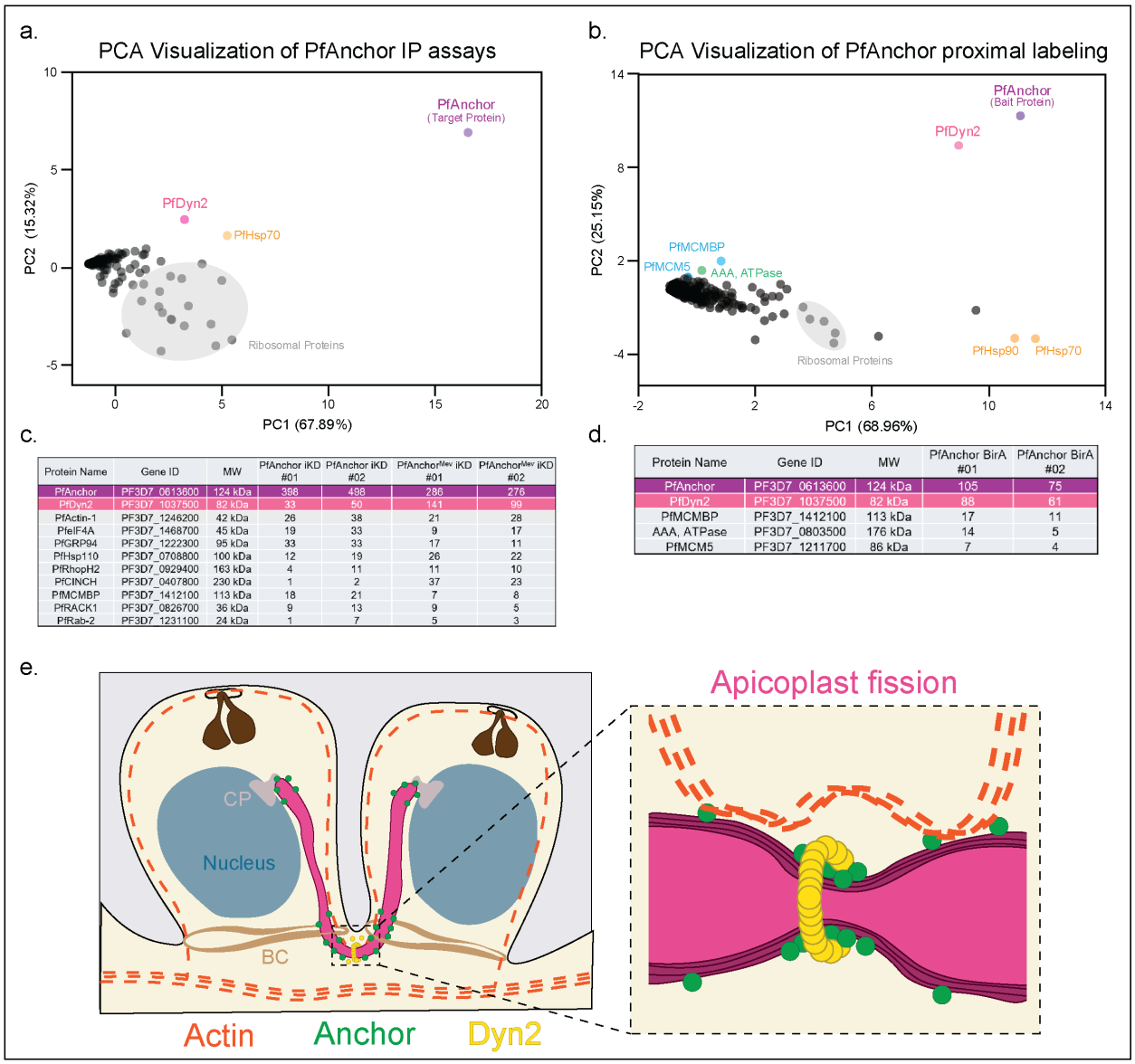

c.

Protein Name	Gene ID	MW	PfAnchor iKD #01	PfAnchor iKD #02	PfAnchor^{Mev} iKD #01	PfAnchor^{Mev} iKD #02
PfAnchor	PF3D7_0613600	124 kDa	398	498	286	276
PfDyn2	PF3D7_1037500	82 kDa	33	50	141	99
PfActin-1	PF3D7_1246200	42 kDa	26	38	21	28
PfeIF4A	PF3D7_1468700	45 kDa	19	33	9	17
PfGRP94	PF3D7_1222300	95 kDa	33	33	17	11
PfHsp110	PF3D7_0708800	100 kDa	12	19	26	22
PfRhopH2	PF3D7_0929400	163 kDa	4	11	11	10
PfCINCH	PF3D7_0407800	230 kDa	1	2	37	23
PfMCMBP	PF3D7_1412100	113 kDa	18	21	7	8
PfRACK1	PF3D7_0826700	36 kDa	9	13	9	5
PfRab-2	PF3D7_1231100	24 kDa	1	7	5	3

d.

Protein Name	Gene ID	MW	PfAnchor BirA #01	PfAnchor BirA #02
PfAnchor	PF3D7_0613600	124 kDa	105	75
PfDyn2	PF3D7_1037500	82 kDa	88	61
PfMCMBP	PF3D7_1412100	113 kDa	17	11
AAA, ATPase	PF3D7_0803500	176 kDa	14	5
PfMCM5	PF3D7_1211700	86 kDa	7	4

Figure 6: PfAnchor interacts with the dynamin-like GTPase PfDyn2, supporting a role in apicoplast division.

a. Principal component analysis (PCA) of mass spectrometry data from PfAnchor immunoprecipitation (IP) assays, performed in biological duplicates using the PfAnchor iKD and PfAnchor^{Mev} iKD cell lines (as listed in c). PfDyn2 is identified as the primary interacting partner of PfAnchor, while PfHsp70 is also detected as a potential secondary interactor. Ribosomal proteins (gray) cluster separately as background. **b.** PCA of PfAnchor proximity labeling (BioID) mass spectrometry data. PfDyn2 is enriched in close proximity to PfAnchor, supporting its interaction. Additionally, components of the MCM complex are detected, though their functional relevance remains unclear. Tables listing proteins uniquely identified in PfAnchor IP (c) and PfAnchor BioID (d) datasets compared to control samples. PfDyn2 is consistently enriched across both methods, further supporting its role as the primary interactor of PfAnchor. **e.** Model of PfAnchor's role in

apicoplast division and inheritance. **Left:** During cytokinesis, the apicoplast (pink) is positioned adjacent to the centriolar plaque (CP) and basal complex (BC), where PfAnchor (green) localizes along the apicoplast membrane. PfDyn2 (yellow) is recruited to the fission site, potentially through PfAnchor, while actin (dashed orange lines) forms a dynamic network [55] that may contribute to membrane remodeling and organelle segregation. **Right:** Close-up view of apicoplast fission, where PfDyn2 assembles at the division site, driving membrane constriction. PfAnchor may function as a tethering factor, linking the fission machinery to the apicoplast membrane and ensuring proper inheritance of the organelle by daughter parasites.